
KNOWLEDGE TRANSFER FROM SIMPLE TO COMPLEX: A SAFE AND EFFICIENT REINFORCEMENT LEARNING FRAMEWORK FOR AUTONOMOUS DRIVING DECISION-MAKING

Rongliang Zhou¹, Jiakun Huang¹, Mingjun Li¹, Hepeng Li¹, Haotian Cao²*, Xiaolin Song¹*

¹ State Key Laboratory of Advanced Design and Manufacturing Technology for Vehicle, Hunan University

² College of Intelligence Science and Technology, National University of Defense Technology

ABSTRACT

A safe and efficient decision-making system is crucial for autonomous vehicles. However, the complexity of driving environments limits the effectiveness of many rule-based and machine learning approaches. Reinforcement Learning, with its robust self-learning capabilities and environmental adaptability, offers a promising solution to these challenges. Nevertheless, safety and efficiency concerns during training hinder its widespread application. To address these concerns, we propose a novel RL framework, Simple to Complex Collaborative Decision (S2CD). First, we rapidly train the teacher model in a lightweight simulation environment. In the more complex and realistic environment, the teacher intervenes when the student agent exhibits suboptimal behavior by assessing actions' value to avert dangers. We also introduce an RL algorithm called Adaptive Clipping Proximal Policy Optimization (ACPPO), which combines samples from both teacher and student policies and employs dynamic clipping strategies based on sample importance. This approach improves sample efficiency while effectively alleviating data imbalance. Additionally, we employ the Kullback-Leibler divergence as a policy constraint, transforming it into an unconstrained problem with the Lagrangian method to accelerate the student's learning. Finally, a gradual weaning strategy ensures that the student learns to explore independently over time, overcoming the teacher's limitations and maximizing performance. Simulation experiments in highway lane-change scenarios show that the S2CD framework enhances learning efficiency, reduces training costs, and significantly improves safety compared to state-of-the-art algorithms. This framework also ensures effective knowledge transfer between teacher and student models, even with a suboptimal teacher, the student achieves superior performance, demonstrating the robustness and effectiveness of S2CD.

Keywords Autonomous Vehicle · Reinforcement Learning · Knowledge Transfer · Teacher-Student Framework · Adaptive Clipping

1 Introduction

Due to the complexity and unpredictability of driving environments, approximately 94% of traffic accidents are related to suboptimal decisions made by human drivers (Alvaro et al., 2018). Suboptimal driving decisions not only compromise traffic safety but also reduce overall traffic efficiency (Lee et al., 2004). Hopefully, the rapid advancement of autonomous driving technology has attracted significant attention due to its potential to improve both traffic safety and efficiency. Autonomous driving systems generally consist of a perception layer, a decision-making layer, and a planning and control layer, in which the decision-making layer commonly referred to as the "brain" of the system (Chen et al., 2017). Ensuring the safety and accuracy of decision-making algorithms is therefore essential for the overall performance of autonomous driving systems (Li et al., 2017). Currently, decision-making methods for autonomous

*Corresponding author

Email addresses: zhourongliang@hnu.edu.cn (Rongliang Zhou), hjk0517@hnu.edu.cn (Jiakun Huang), mingjun1@hnu.edu.cn (Mingjun Li), lhphnu@hnu.edu.cn (Hepeng Li), caohaotian@nudt.edu.cn (Haotian Cao), jqysx1@hnu.edu.cn (Xiaolin Song)

vehicles are generally classified into two categories: knowledge-driven and data-driven. Knowledge-driven methods, such as Hierarchical State Machines (HSM) (Patz et al., 2008), Expert Systems (ES) (Ferguson et al., 2008), and Finite State Machines (FSM) (Buehler et al., 2009), are known for their rigorous logic and high interpretability (Bae et al., 2020). However, these methods are limited by their strong reliance on existing knowledge, which restricts their ability to handle novel or unexpected scenarios (Bianco-Vega et al., 2005; Mozina et al., 2008). In contrast, data-driven methods such as End-to-End (E2E) Learning (Bojarski et al., 2016), Imitation Learning (IL) (Hawke et al., 2020), and Reinforcement Learning (RL) (Sallab et al., 2017; Zhang et al., 2022c) have gained prominence due to their robust self-learning capabilities and adaptability to dynamic environments. RL algorithms, in particular, optimize driving strategies through real-time interactions with the environment, making them highly effective in complex scenarios (Zhu and Zhao, 2021). While RL has demonstrated success in fields such as game artificial intelligence (AI) (Zhang et al., 2022a; Ye et al., 2020), financial transactions (Tsantekidis et al., 2023; Pendharkar and Cusatis, 2018), and energy management (Yu et al., 2019; Kuznetsova et al., 2013), its application in safety-critical areas like autonomous driving and robotic control faces significant challenges due to safety risks and training inefficiency (Liu et al., 2022; Ou et al., 2024).

RL, much like human behavior, can autonomously explore environments and optimize strategies based on environmental feedback (Subramanian et al., 2022). However, traditional RL algorithms inevitably face risks during exploration, often encountering dangers before learning how to avoid them (Chow et al., 2018). The cost of allowing a vehicle to undertake dangerous actions in real-world scenarios is prohibitively high, making it challenging to apply traditional RL algorithms in autonomous driving. In human learning, particularly in hazardous situations, we do not rely solely on trial and error to acquire knowledge (Peng et al., 2022b). Instead, we seek guidance from a teacher to ensure safety and efficiency during the learning process. The teacher not only demonstrates correct actions when necessary but also directly corrects the student's mistakes to avert dangerous situations. For instance, a driving instructor can take control of a vehicle when a novice driver makes an unsafe decision, thereby preventing accidents. Consequently, numerous researchers have incorporated the Teacher-Student Framework (TSF) (Zimmer et al., 2014; Liu et al., 2023) into RL, enabling student agents to safely and efficiently navigate complex scenarios through autonomous exploration and teacher guidance. In the TSF, a high-performance neural network or human expert acts as the teacher, intervening when the student's actions meet specific criteria. When an intervention occurs, the teacher's actions replace the student's actions in the replay buffer as training data, which is later used to optimize the student's model via RL algorithms. However, human-in-the-loop TSF requires continuous expert monitoring, which is labor-intensive, and the effectiveness of human teachers can be influenced by subjective factors like emotions and mental state. To overcome these issues, most TSF approaches rely on pre-training a high-performance teacher model using neural networks, allowing the student to learn correct behaviors from the teacher's demonstrations. Yet, in fields like robotic control and autonomous driving, obtaining such a high-performance teacher in advance can be extremely expensive. Furthermore, in current TSF methods, if the teacher provides suboptimal demonstrations, the student may learn incorrect strategies, limiting its performance (Xue et al., 2023). Another limitation of current TSF methods is that the RL algorithm can only utilize the Markov Decision Process (MDP) corresponding to the action chosen by either the teacher or the student at each step, leading to significant data wastage since alternative actions are not leveraged.

In summary, traditional RL algorithms involve high training costs but fail to guarantee the safety of agents during training. While standard TSF methods help student agents learn safely and efficiently, they come with significant costs in developing a high-performance teacher, and the student's ultimate performance is constrained by the teacher's abilities. Furthermore, these methods cannot optimize the policy by simultaneously utilizing samples generated by both the teacher and student models. To address these limitations, this paper introduces a novel TSF framework called Simple to Complex Collaborative Decision (S2CD), which enhances knowledge transfer between teacher and student. Unlike other TSFs, the S2CD framework accelerates training by first training the teacher model in a lightweight simulation environment with similar scenarios, then guiding the student in more complex simulations or real-world settings. We also theoretically demonstrated that teacher guidance improves both the performance and safety ceilings of the student during training. Additionally, we enhance the Proximal Policy Optimization (PPO) algorithm and propose Adaptive Clipping PPO (ACPPO), which utilizes data from both teacher and student models, significantly improving sample efficiency and alleviating data imbalance. The algorithm adaptively adjusts the clipping factor based on sample importance, boosting learning efficiency. During the policy optimization process, the neural network is updated by constraining the Kullback-Leibler (KL) divergence between the teacher's and student's policies, facilitating the rapid convergence of the student policy to the teacher's. Finally, S2CD employs a weaning strategy that allows the student agent to independently explore the environment in later training stages, thus overcoming the teacher's limitations. The main contributions of this paper are summarized as follows:

- This paper presents a novel TSF called S2CD, which accelerates the training of a teacher model in a lightweight simulation environment and uses it to guide the student agent in learning safely and efficiently in more complex simulated or real-world environments.

- This paper proposes the ACPPO algorithm, integrated within the S2CD framework, which simultaneously utilizes data from both teacher and student models while adaptively adjusting the clipping factor based on sample importance, thus enhancing sample efficiency and alleviating data imbalance.
- This paper introduces the use of the KL divergence between the teacher's and student's policies as a constraint during policy updates, transforming it into an unconstrained problem using the Lagrangian method to facilitate the rapid convergence of the student's policy to the teacher's.
- This paper investigates intervention and weaning strategies within the S2CD framework, where teacher interventions are triggered based on action values, and the frequency of interventions is gradually reduced to promote the student's independent exploration, mitigating the limitations imposed by suboptimal teacher performance.

Section 2 reviews related work and analyzes the strengths and weaknesses of these studies to underscore the value of our research. **Section 3** elaborates on the theoretical foundation of the PPO algorithm and the principles of the ACPPO algorithm before introducing the S2CD decision-making framework. This framework comprises an offline learning-based teacher training module, an ACPPO-based high-level decision-making layer, a cubic spline interpolation-based path planning layer, and a PID algorithm-based control layer. **Section 4** provides a detailed explanation of the differences between the Highway-Env and Carla simulation environments, as well as the implementation details of the simulation experiments, including scenario specification, scene modeling, and simulation settings. **Section 5** presents the simulation results of the S2CD framework and compares them with other mainstream algorithms. **Section 6** concludes the paper and then explores the study's limitations and directions for future research.

2 Related Works

The central idea of this work is to facilitate the safe and efficient learning of RL agents through a knowledge transfer technique based on the TSF. Therefore, this section reviews studies related to knowledge transfer and Safe RL, analyzing their strengths and weaknesses to highlight the innovative aspects and practical significance of this research.

2.1 Knowledge Transfer

While RL has been widely applied across various fields and has demonstrated impressive results, most research has primarily focused on simulation experiments. However, in the context of autonomous driving, the ultimate goal is real-world application, where safety and efficiency during training process are critical factors in assessing algorithm performance. Training standard RL algorithms on real vehicles would not only risk substantial damage but also incur significant time costs. Knowledge transfer seeks to improve the learning efficiency of models by transferring knowledge from previously learned tasks to new tasks. By leveraging existing policies or experiences, the new task can accelerate the learning process, thereby reducing the need for extensive data collection or large sample sizes. This technique is especially valuable in environments where acquiring training data is costly or time-consuming. Consequently, effectively transferring knowledge from simulation-based training to agents operating in real-world or more complex simulation environments has become a significant focus of research.

For example, [Qiao et al. \(2018\)](#) and [Song et al. \(2021\)](#) employed Curriculum Learning (CL) strategies to achieve notable performance in urban intersection and overtaking tasks, respectively. CL enhances model learning effectiveness by gradually increasing task difficulty, instead of requiring models to tackle complex tasks directly ([Bengio et al., 2009](#)). However, CL requires meticulously designed multi-level tasks. Furthermore, the progression from simpler to more complex tasks can increase training time and computational resource demands. Transfer Learning (TL) is another knowledge transfer technique that effectively reduces the training costs of the target task by applying knowledge acquired from the source task to the target task. For instance, [Shu et al. \(2021\)](#) combined RL with TL to transfer decision-making knowledge from one driving task to another in an intersection environment. Similarly, [Akhauri et al. \(2020\)](#) utilized simulated accident data for TL, enabling the model to generalize more rapidly and effectively to real-world scenarios. However, if the source and target tasks are not sufficiently related, the performance of TL may deteriorate, potentially resulting in "negative transfer" ([Zhang et al., 2022b](#)). Another approach to knowledge transfer is the use of Digital Twins (DT). By creating an accurate digital replica of a physical entity or system, we can map data from the physical world to the virtual world ([Niaz et al., 2021](#)), enabling real-time monitoring, simulation, analysis, and optimization of physical entities. [Voogd et al. \(2023\)](#) employed DT technology to combine virtual and real-world data on vehicle dynamics and traffic scenarios, effectively bridging the gap between simulation and reality. [Wang et al. \(2024\)](#) designed and implemented an E2E DT system for autonomous driving. This system captures real-world traffic information, processes it in the cloud to create a digital twin model, and then utilizes this model to provide route planning services for autonomous vehicles. Despite DT technology effectively bridging the gap between simulation training

and real-world applications, accurate simulation processes remain indispensable. Designing simulation programs that accurately mirror or fully replicate real-world conditions is both challenging and costly (Yun and Park, 2021). Moreover, pre-training a high-performance model in a high-fidelity simulation environment is resource-intensive.

Therefore, a key area of research focuses on developing methods to train models quickly and efficiently in simplified simulation environments. Subsequently, effective knowledge transfer techniques are applied to enable agents to complete training safely and effectively in more complex simulations or real-world environments.

2.2 Safe RL

RL methods can enhance an agent's ability to avoid dangers by learning from previous training failures and developing efficient behavioral strategies to adapt to complex environments. However, the application of these methods in safety-critical domains continues to present substantial safety challenges (Garcia and Fernández, 2015). Ensuring policy safety throughout the training process and preventing agents from encountering dangerous situations are key to expanding the applicability of RL to more fields. Safe RL seeks to ensure that RL models avoid unsafe behaviors during both training and execution, particularly in high-risk or safety-critical domains such as autonomous driving. Safe RL techniques focus on balancing the exploration of novel strategies with the imperative to maintain safety, ensuring that the learned policies adhere to required safety standards throughout the learning process. Consequently, many researchers are focusing on incorporating constrained optimization, hard rule constraints, and risk assessment into RL algorithms to mitigate unsafe behaviors during both the learning and execution phases.

For instance, methods like PPO-Lag (Stooke et al., 2020) and SAC-Lag (Ha et al., 2021) utilize the Lagrangian method, which simultaneously updates both the policy and the Lagrange multiplier through primal-dual optimization, thereby transforming the safety-constrained optimization problem into an unconstrained one. Peng et al. (2022a) proposed the Separated Proportional Integral Lagrangian (SPIL) algorithm, which mitigates oscillations and reduces conservatism in RL policies during car-following scenarios. Zhang et al. (2024) introduced cognitive uncertainty as a constraint in Lagrangian Safe RL algorithms, aiming to enhance both exploration and safety performance in autonomous vehicles. While the Lagrangian method is effective in handling safety constraints, it lacks a clear mechanism to prevent hazardous events (Li et al., 2022b). Thus, agents may still engage in unsafe exploration during training. Consequently, many researchers have applied rule-based constraints (Cao et al., 2022; Likmeta et al., 2020) or risk estimation methods (Mo et al., 2021; Li et al., 2022a) to Safe RL in autonomous driving, aiming to ensure a minimum level of policy safety performance. Although these methods can prevent a significant number of unsafe actions, their effectiveness heavily depends on the quality of the rule design or risk assessment models. To further reduce unsafe events, researchers have shifted their focus toward Safe RL approaches based on the TSF. Within the TSF, teacher policies can be classified into human expert strategies and well-trained neural network strategies. For example, Wu et al. (2023) and Huang et al. (2024) employed human experts to mentor AI agents. During the student agent's interaction with the environment, the human expert intervenes in dangerous situations and demonstrates the correct actions, thereby ensuring driving safety throughout the student's training process. While Safe RL methods involving human expert intervention significantly improve the safety of the exploration process, they incur high labor costs. Moreover, the teaching performance of human experts is highly influenced by subjective factors, leading to instability in the final model performance. To reduce labor costs, many researchers have employed well-trained neural network models as "teachers" to guide student agents during the learning process. For instance, Peng et al. (2022b) and Xue et al. (2023) employed RL algorithms to obtain a well-trained teacher model, when the conditions defined by a switching function, which determines whether to intervene, are met, the teacher takes over the student's actions to demonstrate correct operations and avoid dangerous situations. Zhou et al. (2024) employed the SOAR cognitive architecture as a teacher to guide the student agent toward efficient and safe learning, while also offering a certain degree of interpretability.

Model-based TSF eliminates the need for real-time monitoring by human experts but incurs the cost of training a high-performance model. Moreover, the student's final performance is limited by the teacher's capabilities. Therefore, although TSF can maximize agent safety during training and improve learning efficiency, these methods have not yet been widely adopted in the field of autonomous driving.

3 Theoretical Background

In this section, we provide a comprehensive explanation of the technical background underlying the S2CD framework. First, we present the theoretical foundations of the PPO algorithm. Subsequently, we refine the clipping strategy of the PPO algorithm, introducing the ACPPO algorithm. Lastly, we incorporate ACPPO into the S2CD framework and offer a detailed description of the components within the S2CD framework.

3.1 Proximal Policy Optimization Algorithm

DRL achieves its goals through interactions between an agent and its environment, and it can be broadly categorized into two main approaches: value-based methods and policy-based methods. The fundamental principle of value-based methods is to learn a value function that estimates the long-term returns for each state or state-action pair. The optimal action is then selected based on this value function. In contrast, policy-based methods directly optimize a policy that maps states to actions, making decisions based on the probabilistic distribution of this policy. Although value-based methods perform adequately in simpler tasks, their efficiency decreases significantly as the complexity of the state or action space increases. Conversely, policy-based DRL methods offer a well-defined optimization path that ensures convergence to a stable policy while enhancing exploration through the learning of stochastic policies. In high-dimensional and complex task environments, policy-based methods are typically more appropriate and offer superior scalability. Therefore, this paper will focus on policy-based DRL methods.

The objective of DRL is to identify a policy $\pi(a|s)$ that maximizes the cumulative discounted reward across all time steps, defined as:

$$G_t = \sum_{k=0}^{\infty} \gamma^k r_{t+k} \quad (1)$$

where r_t represents the reward received at time step t , and $\gamma \in [0, 1)$ is the discount factor, which determines the importance of future rewards. In policy gradient methods, the objective is to optimize the policy $\pi(a|s)$ to maximize the expected cumulative reward, expressed as:

$$J(\theta) = \mathbb{E}_{s_0} [V^{\pi_\theta}(s_0)] = \mathbb{E}_{\pi_\theta} \left[\sum_{t=0}^{\infty} \gamma^t r(s_t, a_t) \right] \quad (2)$$

where \mathbb{E} is the expectation operator for a finite batch of samples, π_θ denotes the current policy, with θ representing its parameters. The state value function $V^\pi(s_t) = \mathbb{E}_\pi \left[\sum_{k=0}^{\infty} \gamma^k r(s_{t+k}, a_{t+k}) | s_t \right]$ represents the expected return when starting from state s_t under policy π_θ .

The optimization objective under the policy π_θ , denoted as $J(\theta)$, can be expressed in the expected form of the new policy $\pi_{\theta'}$:

$$\begin{aligned} J(\theta) &= \mathbb{E}_{s_0} [V^{\pi_\theta}(s_0)] \\ &= \mathbb{E}_{\pi_{\theta'}} \left[\sum_{t=0}^{\infty} \gamma^t V^{\pi_\theta}(s_t) - \sum_{t=1}^{\infty} \gamma^t V^{\pi_\theta}(s_t) \right] \\ &= -\mathbb{E}_{\pi_{\theta'}} \left[\sum_{t=0}^{\infty} \gamma^t (\gamma V^{\pi_\theta}(s_{t+1}) - V^{\pi_\theta}(s_t)) \right] \end{aligned} \quad (3)$$

According to above equations and Paper [Kakade and Langford \(2002\)](#), we can deduce the gap between the objective function of the new policy $\pi_{\theta'}$ and the current policy π_θ :

$$\begin{aligned} J(\theta') - J(\theta) &= \mathbb{E}_{s_0} [V^{\pi_{\theta'}}(s_0)] - \mathbb{E}_{s_0} [V^{\pi_\theta}(s_0)] \\ &= \mathbb{E}_{\pi_{\theta'}} \left[\sum_{t=0}^{\infty} \gamma^t r(s_t, a_t) \right] + \mathbb{E}_{\pi_{\theta'}} \left[\sum_{t=0}^{\infty} \gamma^t (\gamma V^{\pi_\theta}(s_{t+1}) - V^{\pi_\theta}(s_t)) \right] \\ &= \mathbb{E}_{\pi_{\theta'}} \left[\sum_{t=0}^{\infty} \gamma^t (r(s_t, a_t) + \gamma V^{\pi_\theta}(s_{t+1}) - V^{\pi_\theta}(s_t)) \right] \end{aligned} \quad (4)$$

Meanwhile, the advantage function is denoted as:

$$\begin{aligned} A^{\pi_\theta}(s_t, a_t) &= Q^{\pi_\theta}(s_t, a_t) - V^{\pi_\theta}(s_t) \\ &= r(s_t, a_t) + \gamma V^{\pi_\theta}(s_{t+1}) - V^{\pi_\theta}(s_t) \end{aligned} \quad (5)$$

where $Q^\pi(s_t, a_t) = r(s_t, a_t) + \gamma \mathbb{E}_{s_{t+1}} [V^\pi(s_{t+1})]$ is the state-action value function, representing the expected return after taking action a_t in state s_t , so:

$$\begin{aligned} J(\theta') - J(\theta) &= \mathbb{E}_{\pi_{\theta'}} \left[\sum_{t=0}^{\infty} \gamma^t A^{\pi_\theta}(s_t, a_t) \right] \\ &= \sum_{t=0}^{\infty} \gamma^t \mathbb{E}_{s_t \sim P_t^{\pi_{\theta'}}} \mathbb{E}_{a_t \sim \pi_{\theta'}(\cdot | s_t)} [A^{\pi_\theta}(s_t, a_t)] \end{aligned} \quad (6)$$

where $P_t^\pi(s)$ is the density function of state at time t . Let $\nu^\pi(s) = (1 - \gamma) \sum_{t=0}^{\infty} \gamma^t P_t^\pi(s)$ represent the discounted visitation frequencies of states, so:

$$\begin{aligned} J(\theta') - J(\theta) &= \frac{1}{1 - \gamma} \sum_s \nu^{\pi_{\theta'}}(s) \sum_a \pi_{\theta'}(a|s) A^{\pi_\theta}(s, a) \\ &= \frac{1}{1 - \gamma} \mathbb{E}_{s \sim \nu^{\pi_{\theta'}}} \mathbb{E}_{a \sim \pi_{\theta'}(\cdot|s)} [A^{\pi_\theta}(s, a)] \end{aligned} \quad (7)$$

Therefore, as long as we can find a new policy such that $\mathbb{E}_{s \sim \nu^{\pi_{\theta'}}} \mathbb{E}_{a \sim \pi_{\theta'}(\cdot|s)} [A^{\pi_\theta}(s, a)] \geq 0$, we can ensure that the policy performance improves monotonically, i.e., $J(\theta') \geq J(\theta)$.

[Eq. 7](#) contains $\nu^{\pi_{\theta'}}(s)$, which results from the interaction between the new policy $\pi_{\theta'}$ and the environment. However, $\pi_{\theta'}$ is the exact policy we need to solve. To address this, we replace $\nu^{\pi_\theta}(s)$ with $\nu^{\pi_{\theta'}}(s)$ in the total discounted rewards function $J(\theta)$. Thus, the local approximate objective function is obtained:

$$\begin{aligned} L_\theta(\theta') &= J(\theta) + \frac{1}{1 - \gamma} \sum_s \nu^{\pi_\theta}(s) \sum_a \pi_{\theta'}(a|s) A^{\pi_\theta}(s, a) \\ &= J(\theta) + \frac{1}{1 - \gamma} \mathbb{E}_{s \sim \nu^{\pi_\theta}} \mathbb{E}_{a \sim \pi_{\theta'}(\cdot|s)} [A^{\pi_\theta}(s, a)] \end{aligned} \quad (8)$$

Since $J(\theta) = \mathbb{E}_{\pi_\theta} [\sum_{t=0}^{\infty} \gamma^t r(s_t, a_t)]$, only the second term in [Eq. 8](#) is related to optimizing the policy $\pi_{\theta'}$. We employ the importance sampling method to handle the action distribution, resulting in the following surrogate optimization objective function:

$$\begin{aligned} L_\theta(\theta') &= \mathbb{E}_{s \sim \nu^{\pi_\theta}} \mathbb{E}_{a \sim \pi_{\theta'}(\cdot|s)} [A^{\pi_\theta}(s, a)] \\ &= \mathbb{E}_{s \sim \nu^{\pi_\theta}} \mathbb{E}_{a \sim \pi_\theta(\cdot|s)} \left[\frac{\pi_{\theta'}(a|s)}{\pi_\theta(a|s)} A^{\pi_\theta}(s, a) \right] \end{aligned} \quad (9)$$

Hence, we can estimate and optimize the new policy $\pi_{\theta'}$ using data sampled from the old policy π_θ . To ensure that the objective function meets the necessary conditions, [Schulman et al. \(2015\)](#) derived the following performance bounds:

Theorem 1. Define that $C = 4\gamma \max_{s,a} |A^{\pi_\theta}(s, a)| / (1 - \gamma)^2$, $D_{KL}^s(\pi_\theta, \pi_{\theta'}) \triangleq D_{KL}(\pi_\theta(\cdot|s) \parallel \pi_{\theta'}(\cdot|s))$, $D_{KL}^{max}(\pi_\theta, \pi_{\theta'}) \triangleq \max_{s \in S} D_{KL}^s(\pi_\theta, \pi_{\theta'})$, $M_\theta(\theta') = L_\theta(\theta') - CD_{KL}^{max}(\pi_\theta, \pi_{\theta'})$. We have $J(\theta') \geq M_\theta(\theta')$, $J(\theta) = M_\theta(\theta)$.

This theorem indicates that by maximizing $M_\theta(\theta')$, the performance of the new policy $\pi_{\theta'}$ is guaranteed to be non-decreasing. However, due to the deep architecture of the policy network, using an excessively large step size when optimizing $L_\theta(\theta')$ along the policy gradient can lead to substantial changes in the policy, potentially resulting in overshooting and negatively impacting performance. To address this issue, [Schulman et al. \(2015\)](#) proposed Trust Region Policy Optimization (TRPO), which optimizes $L_\theta(\theta')$ with a constraint on the KL divergence, $D_{KL}^{max}(\pi_\theta, \pi_{\theta'}) \leq \delta$, between the old and new policies. To simplify the computation, the average KL divergence can be used to relax the constraint on the maximum value of the KL divergence. The final simplified surrogate optimization objective for the TRPO algorithm is:

$$\begin{aligned} \max_{\theta'} L_\theta(\theta') \\ \text{s.t.} \mathbb{E}_{s \sim \nu^{\pi_\theta}} [D_{KL}(\pi_\theta(\cdot|s), \pi_{\theta'}(\cdot|s))] \leq \delta \end{aligned} \quad (10)$$

However, TRPO is computationally complex and inefficient. To address this, [Schulman et al. \(2017\)](#) proposed the PPO algorithm, which replaces the KL divergence constraint in TRPO with a direct maximization of the clipped surrogate objective function:

$$L^{CLIP}(\theta) = \mathbb{E}_{\pi_\theta} [\min(r_t(\theta) A^{\pi_\theta}(s, a), \text{clip}(r_t(\theta), 1 - \epsilon, 1 + \epsilon) A^{\pi_\theta}(s, a))] \quad (11)$$

where the probability ratio $r_t(\theta) = \frac{\pi_{\theta'}(a_t|s_t)}{\pi_\theta(a_t|s_t)}$ is clipped within the range $(1 - \epsilon, 1 + \epsilon)$ using the operator clip , defined as $\text{clip}(r_t(\theta), 1 - \epsilon, 1 + \epsilon) = \min(\max(r_t(\theta), 1 - \epsilon), 1 + \epsilon)$, where ϵ is a hyperparameter that represents the clipping range. The minimization operation ensures that [Eq. 11](#) serves as the lower bound of [Eq. 9](#).

3.2 Adaptive Clipping Proximal Policy Optimization Algorithm

Although the clipping mechanism in the PPO algorithm provides an effective and reliable strategy for policy updates, a fixed clipping factor ϵ may not adaptively improve learning performance based on the significance of each sample, particularly when the samples are come from different sources. To address this issue, we propose an improved PPO algorithm called ACPPO. This algorithm incorporates an adaptive clipping mechanism, allowing for automatic adjustment of the clipping factor based on the importance of the samples. When encountering more significant samples, the algorithm permits larger updates to the policy parameters, while constraining changes to the policy parameters for less critical samples.

First, we analyze the clipping mechanism of the PPO algorithm and establish its relationship with the objective constraints. Based on [Eq. 7](#) and [Eq. 9](#), we derive the following:

$$\begin{aligned}
J(\theta') - J(\theta) &= \frac{1}{1-\gamma} \mathbb{E}_{s \sim \nu^{\pi_{\theta'}}} \mathbb{E}_{a \sim \pi_{\theta'}(\cdot|s_t)} [A^{\pi_{\theta}}(s, a)] \\
&= \frac{1}{1-\gamma} L_{\theta}(\theta') + \frac{1}{1-\gamma} [\mathbb{E}_{s \sim \nu^{\pi_{\theta'}}} \mathbb{E}_{a \sim \pi_{\theta'}(\cdot|s_t)} [A^{\pi_{\theta}}(s, a)] - \mathbb{E}_{s \sim \nu^{\pi_{\theta}}} \mathbb{E}_{a \sim \pi_{\theta'}(\cdot|s_t)} [A^{\pi_{\theta}}(s, a)]] \\
&\geq \frac{1}{1-\gamma} L_{\theta}(\theta') - \frac{1}{1-\gamma} \left| \sum_{s,a} [\nu^{\pi_{\theta'}}(s) - \nu^{\pi_{\theta}}(s)] \times \pi_{\theta'}(a|s) A^{\pi_{\theta}}(s, a) \right| \\
&= \frac{1}{1-\gamma} L_{\theta}(\theta') - \frac{1}{1-\gamma} \left| \sum_s [\nu^{\pi_{\theta'}}(s) - \nu^{\pi_{\theta}}(s)] \times \sum_a \pi_{\theta'}(a|s) A^{\pi_{\theta}}(s, a) \right|
\end{aligned} \tag{12}$$

We define that $\Delta \nu_{\pi_{\theta}}^{\pi_{\theta'}} \cdot A_{\pi_{\theta}}^{\pi_{\theta'}} \triangleq \sum_s [\nu^{\pi_{\theta'}}(s) - \nu^{\pi_{\theta}}(s)] \times \sum_a \pi_{\theta'}(a|s) A^{\pi_{\theta}}(s, a)$, and bound it by Hölder's inequality:

$$\begin{aligned}
|\Delta \nu_{\pi_{\theta}}^{\pi_{\theta'}} \cdot A_{\pi_{\theta}}^{\pi_{\theta'}}| &\leq \sum_s |[\nu^{\pi_{\theta'}}(s) - \nu^{\pi_{\theta}}(s)]| \max_{s,a} |A^{\pi_{\theta}}(s, a)| \\
&\leq \frac{\gamma}{1-\gamma} \max_{s,a} |A^{\pi_{\theta}}(s, a)| \sum_s \nu^{\pi_{\theta}}(s) \sum_a |\pi_{\theta'}(a|s) - \pi_{\theta}(a|s)| \\
&= \frac{\gamma}{1-\gamma} \max_{s,a} |A^{\pi_{\theta}}(s, a)| \mathbb{E}_{s \sim \nu^{\pi_{\theta}}} \mathbb{E}_{a \sim \pi_{\theta}(\cdot|s_t)} \left[\frac{\pi_{\theta'}(a|s)}{\pi_{\theta}(a|s)} - 1 \right] \\
&= \frac{\gamma}{1-\gamma} \max_{s,a} |A^{\pi_{\theta}}(s, a)| \mathbb{E}_{s \sim \nu^{\pi_{\theta}}} \mathbb{E}_{a \sim \pi_{\theta}(\cdot|s_t)} [r_t(\theta) - 1]
\end{aligned} \tag{13}$$

Thus, we can get the following improvement lower bound for policy as stated in [Theorem 2](#):

Theorem 2. *For the current policy $\pi_{\theta'}$ and the old policy π_{θ} , we have:*

$$J(\theta') - J(\theta) \geq \frac{1}{1-\gamma} L_{\theta}(\theta') - C \cdot \mathbb{E}_{s \sim \nu^{\pi_{\theta}}} \mathbb{E}_{a \sim \pi_{\theta}(\cdot|s_t)} |r_t(\theta) - 1| \tag{14}$$

where C is defined as in [Theorem 1](#).

[Theorem 2](#) demonstrates that the performance deviation between any two successive policies can be constrained by the expected value $\mathbb{E}_{s \sim \nu^{\pi_{\theta}}} \mathbb{E}_{a \sim \pi_{\theta}(\cdot|s_t)} |r_t(\theta) - 1|$, which represents the absolute value of the policy probability deviation. According to [Eq. 11](#), the gradient of the clipped surrogate objective is given by:

$$\nabla_{\theta} L^{CLIP}(\theta) = \mathbb{E}_{\pi_{\theta}} [r_t(\theta) A^{\pi_{\theta}}(s, a) \nabla_{\theta} \log \pi_{\theta}(a_t|s_t) \times \{r_t(\theta) \in (1-\epsilon, 1+\epsilon) \text{ or } \text{sgn}(r_t(\theta) - 1) \neq \text{sgn}(A^{\pi_{\theta}}(s, a))\}] \tag{15}$$

PPO limits the difference between successive policies by eliminating the reward generated when $|r_t(\theta) - 1|$ exceeds the clipping parameter ϵ , while maximizing the surrogate objective. This is achieved by using the clip operator to restrict the values of $r_t(\theta)$ within a fixed range $(1-\epsilon, 1+\epsilon)$, thereby limiting the variation between the new and old policies and ensuring that the variance among samples does not become excessive. The value of the objective function $L^{CLIP}(\theta)$ depends on whether $A^{\pi_{\theta}}$ is positive or negative. If $A^{\pi_{\theta}} > 0$, indicating that the state-action value of a_t is above the average state value, maximizing $L^{CLIP}(\theta)$ increases $r_t(\theta)$, but restricts it to remain below $1+\epsilon$. Conversely, if $A^{\pi_{\theta}} < 0$, meaning the state-action value of a_t is below the average state value, maximizing $L^{CLIP}(\theta)$ decreases $r_t(\theta)$, but restricts it to remain above $1-\epsilon$.

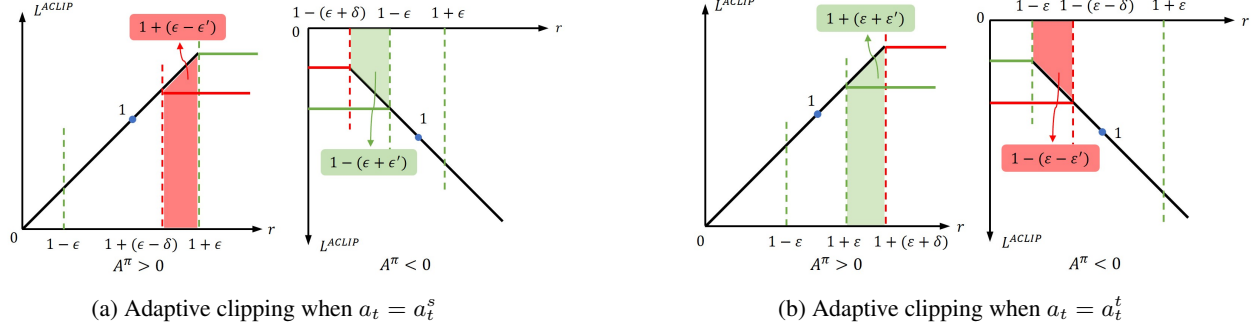


Figure 1: Adaptive clipping range of ACPPO algorithm

From the aforementioned conclusions, it is clear that the use of collected samples to update policies is constrained by the clipping factor ϵ . In traditional PPO algorithms, ϵ is fixed. When encountering samples from different sources, a fixed clipping factor may fail to fully leverage the information from these diverse samples, especially for important ones, limiting the scope of policy updates and resulting in reduced algorithm performance or slower convergence rates. When the student agent interacts with the environment and receives direct interventions on actions from teacher model, the actions collected by the agent in the same state s_t originate from two different sources:

1. The action a_t^s output by the student policy;
2. The action a_t^t output by the teacher policy.

Assuming that the teacher's actions a_t^t are safe and reliable in most cases, we can consider that a_t^t has a greater advantage over a_t^s for the current state s_t . Therefore, a_t^t is more important for agent training. To accommodate samples from different sources, we propose using a dynamically adjusted adaptive clipping factor to better reflect the importance of the samples. The following adjustments are made to the surrogate objective function:

$$L^{ACLIP}(\theta) = \begin{cases} \mathbb{E}_{\pi_\theta} [\min(r_t(\theta) A^{\pi_\theta}(s, a), \text{clip}(r_t(\theta), 1 - (\epsilon + \epsilon'), 1 + (\epsilon - \epsilon')) A^{\pi_\theta}(s, a))] , & \text{if } a_t = a_t^s \\ \mathbb{E}_{\pi_\theta} [\min(r_t(\theta) A^{\pi_\theta}(s, a), \text{clip}(r_t(\theta), 1 - (\epsilon - \epsilon'), 1 + (\epsilon + \epsilon')) A^{\pi_\theta}(s, a))] , & \text{if } a_t = a_t^t \end{cases} \quad (16)$$

where ϵ' is the adaptive factor, determined by the following equation:

$$\epsilon' = \psi \frac{(\pi_\theta(a_t^s|s_t) - \pi_\theta(a_t^t|s_t)) + 1}{2}, \quad 0 \leq \psi \leq \epsilon \quad (17)$$

where ψ is a hyperparameter used to adjust the extent of adaptive clipping, and $\pi_\theta(a_t^s|s_t) - \pi_\theta(a_t^t|s_t)$ represents the difference in the probabilities of policy π_θ outputting a_t^s and a_t^t in state s_t . It should be noted that, in order to maintain the monotonicity of the objective function, the sign of the adjusted clipping factor must not change, so $(\epsilon - \epsilon') \geq 0$.

For a clearer understanding of Eq. 16, we analyze it using Fig. 1. It is evident that when $a_t = a_t^s$, we consider a_t^s to be less advantageous than a_t^t . Therefore, when $A^{\pi_\theta} > 0$, we reduce the upper bound of r_t , decreasing the increment of $\pi_\theta(a_t^s|s_t)$, and the larger the difference $\pi_\theta(a_t^s|s_t) - \pi_\theta(a_t^t|s_t)$, the lower the upper bound of r_t . Conversely, when $A^{\pi_\theta} < 0$, we further lower the lower bound of r_t , making the decrease in $\pi_\theta(a_t^s|s_t)$ more significant, and the larger the difference $\pi_\theta(a_t^s|s_t) - \pi_\theta(a_t^t|s_t)$, the lower the lower bound of r_t . On the other hand, when $a_t = a_t^t$, we consider this action to be more important. Therefore, when $A^{\pi_\theta} > 0$, we further raise the upper bound of r_t , increasing the increment of $\pi_\theta(a_t^t|s_t)$, and the larger the difference $\pi_\theta(a_t^s|s_t) - \pi_\theta(a_t^t|s_t)$, the higher the upper bound of r_t . When $A^{\pi_\theta} < 0$, we raise the lower bound of r_t , reducing the decrement in $\pi_\theta(a_t^t|s_t)$, and the larger the difference $\pi_\theta(a_t^s|s_t) - \pi_\theta(a_t^t|s_t)$, the higher the lower bound of r_t . Through adaptive clipping, the PPO algorithm can better adapt to the importance of different samples, quickly aligning the policy towards the expert policy during training, thus enhancing the learning efficiency of the agent.

3.3 Simple to Complex Collaborative Decision-Making Framework

In this section, we introduce the S2CD framework in detail, which consists of an offline teacher training module, a high-level decision-making layer, and a low-level layer (comprising the path planning and control layers). The teacher training module first generates an autonomous driving teacher model by rapidly training a RL agent in a lightweight simulation environment. During the training of the teacher model, two neural networks are used to fit the Return function and the Q-Value function, respectively, predicting the return values and Q-values for state-action pairs.

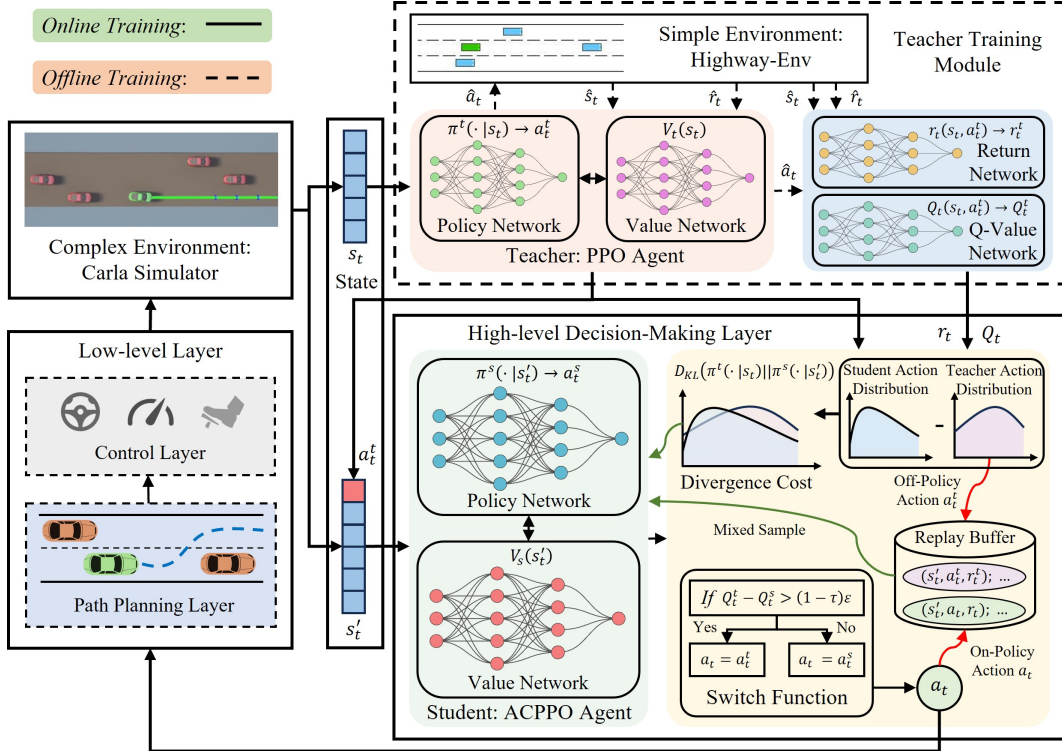


Figure 2: The S2CD decision-making framework consists of a teacher training module, a high-level decision-making layer, and a lower-level layer, enhanced by 4 innovative modules to improve learning efficiency and performance: 1. Employing the teacher model for action intervention and demonstration to enhance the safety of the student policy; 2. Utilizing dual-source data for training to improve sample efficiency; 3. Employing KL divergence constraints in policy updates to enable the student policy to quickly approach the teacher policy; 4. Gradually reducing the teacher model’s intervention via a weaning mechanism to prevent excessive reliance of the student on the teacher.

The high-level decision-making layer utilizes guidance from the teacher model and state information from the perception module to generate high-level commands, which are then transmitted to the low-level layer. The low-level layer is responsible for managing the driving trajectory, including the driving path, lateral speed, and longitudinal speed. Ultimately, the ego vehicle executes actions based on the output values from the low-level layer. While our research primarily focuses on the high-level decision-making layer, the details of the low-level layer are provided in [Section 3.3.3](#). [Fig. 2](#) illustrates the components of the S2CD decision-making framework.

3.3.1 Teacher Training Module

The teacher training module functions as an offline pre-training module. We pre-train the teacher model using the PPO algorithm in the lightweight autonomous driving simulation environment, Highway-env. In Highway-env, due to the significant simplification of the decision-making and control processes for autonomous vehicles, an effective decision model can be easily trained using the PPO algorithm.

Furthermore, the data collected from the interaction between the agent and the environment, including states, actions, and returns, can be used not only to train the PPO algorithm but also to train the Return and Q-Value networks to approximate the state-action’s return function and Q-value function. When training the student agent in the Carla simulation environment, given a state s_t , the teacher model outputs a guiding action a_t^t based on the probability distribution of π^t . The Return and Q-Value networks then predict the short-term reward (Return) and the long-term reward (Q-value) for selecting action a_t^t in state s_t . Thus, the teacher training module can provide not only decision guidance for the current state but also precise quantitative feedback for the student agent. The algorithm flow of the teacher training module is presented in [Algorithm 1](#).

Algorithm 1: Teacher Model Training

Input: Simple Environment State \hat{s}_t
Output: Teacher Action a_t^t , Predicted Return Value r_t^t , and Q-value Q_t^t

```

1 Randomly initialize Actor network  $\hat{NN}_1$  and Critic network  $\hat{NN}_2$  with weights  $\hat{\theta}_1$  and  $\hat{\theta}_2$ 
2 Randomly initialize Return network  $\bar{NN}_1$  and Q-Value network  $\bar{NN}_2$  with weights  $\bar{\varphi}_1$  and  $\bar{\varphi}_2$ 
3 Copy Actor and Critic networks to Actor and Critic target networks respectively:
    $\hat{NN}'_1 \leftarrow \hat{NN}_1, \hat{NN}'_2 \leftarrow \hat{NN}_2, \hat{\theta}'_1 \leftarrow \hat{\theta}_1, \hat{\theta}'_2 \leftarrow \hat{\theta}_2$ 
4 for  $n = 1 : N_{total}$  do
5   for  $t = 1 : T_{epoch}$  do
6     Get action from  $\pi^t$ :  $\hat{a}_t \leftarrow \pi^t(\cdot | \hat{s}_t)$ 
7     Adopt  $\hat{a}_t$  and collect  $(\hat{s}_t, \hat{a}_t, \hat{r}_t, \hat{s}_{t+1})$  into replay buffer  $\hat{B}$ 
8     Compute advantage estimates  $\hat{A}^{\pi_\theta}$ 
9     Compute Q-Value of  $\hat{a}_t$ :  $\hat{Q}_t$ 
10    Collect  $(\hat{s}_t, \hat{a}_t, \hat{r}_t, \hat{Q}_t)$  into replay buffer  $\bar{B}$ 
11  end
12  Update Actor network  $\hat{NN}_1$  and Critic network  $\hat{NN}_2$  using  $\hat{B}$  and  $\hat{A}^{\pi_\theta}$  by maximizing  $L^{CLIP}(\theta)$ :
     $\hat{\theta}'_1^{new}, \hat{\theta}'_1^{new}, \hat{\theta}'_2^{new}, \hat{\theta}'_2^{new} \leftarrow \hat{\theta}_1, \hat{\theta}'_1, \hat{\theta}_2, \hat{\theta}'_2$ 
13  Update Return network  $\bar{NN}_1$  and Q-Value network  $\bar{NN}_2$  using  $\bar{B}$  via gradient descent:  $\bar{\varphi}_1^{new}, \bar{\varphi}_2^{new} \leftarrow \bar{\varphi}_1, \bar{\varphi}_2$ 
14 end

```

3.3.2 High-level Decision-Making Layer

In the high-level decision-making layer, several modifications have been made to the traditional PPO algorithm by incorporating innovative modules designed to enhance learning efficiency and performance.

Action intervention and demonstration First, after completing the offline training of the teacher model, the environment state s_t is fed into the policy network π^t , which generates the probability distribution of the teacher's policy and outputs the action a_t^t with the highest probability (a_t^t considered optimal by the teacher for s_t). Simultaneously, based on the Return network and Q-Value network, the return and Q-value for action a_t^t in the given state s_t are predicted. Next, the teacher's guiding action a_t^t is used as input to the student model, along with the state s_t , to form a new state representation s'_t . The student agent's policy network generates the probability distribution of actions based on s'_t and selects the action a_t^s with the highest probability. At this stage, both the teacher and student models output actions a_t^t and a_t^s , respectively, according to their own policies. To enhance the teacher's guidance of the student and allow for intervention in the student's actions when necessary, we propose a novel switch function based on the Q-values of a_t^t and a_t^s , as shown below:

$$a_t = \begin{cases} a_t^t, & \text{if } Q_t^t - Q_t^s > (1 - \tau)\varepsilon \\ a_t^s, & \text{otherwise} \end{cases} \quad (18)$$

According to this switch function, we can define the mixed behavior policy π^{mix} as follows:

$$\pi^{\text{mix}}(\cdot | s) = \mathcal{T}(s)\pi^t(\cdot | s) + (1 - \mathcal{T}(s))\pi^s(\cdot | s) \quad (19)$$

where $\mathcal{T}(s) = 1$ indicates that the teacher has intervened in the action, and $\mathcal{T}(s) = 0$ means otherwise.

The switch function indicates that the teacher will tolerate the student when the teacher cannot significantly outperform the student in terms of long-term returns. Specifically, when the difference in Q-value between actions a_t^t and a_t^s exceeds the tolerance threshold $(1 - \tau)\varepsilon$, it implies that the student's performance is suboptimal, necessitating intervention by the teacher. Otherwise, the teacher acknowledges the student's performance and refrains from overriding the action. Here, Q-values are predicted by the trained Q-Value network, ε is the tolerance coefficient used to control the extent of the student's reliance on the teacher, and τ is a decay coefficient, where $1 - \tau$ increases the teacher's tolerance, gradually reducing the student's dependence on the teacher. We design the decay coefficient τ as shown in Eq. 20:

$$\tau = \frac{1}{1 + e^{\frac{n_e - q_2}{q_1}}} \quad (20)$$

Table 1: Parameters of S2CD framework

Hyper-parameters	Value	Hyper-parameters	Value
Maximal learning rate	0.0005	Discount factor γ	0.96
Learning rate decay	True	Lambda entropy β	0.01
Total steps of one episode	5,000	Clip parameter ϵ	0.2
Total training steps	300K	Lambda advantage λ	0.98
Optimizer	AdamW	Hyperparameter q_1	3
Mini batch size	64	Hyperparameter q_2	10
Hyperparameter of AC ψ	0.2	Initial Lagrange multiplier ξ	0.01
Efficiency weight α_1	0.5	Safety weight α_2	1.0
Tolerance coefficient ε	0.5		

where n_e is the number of episodes during training, q_1 and q_2 are hyperparameters shown in Table 1. Based on this switch function, the final action a_t , determined for execution, is passed to the low-level layer for vehicle control.

To evaluate the effectiveness of the teacher’s policy intervention, we derive the upper and lower bounds of the return $J_{\theta_{\text{mix}}}$ for the mixed behavior policy, as shown in Theorem 3:

Theorem 3. *With the switch function, the return of the mixed behavior policy $J(\theta_{\text{mix}})$ is bounded both below and above by:*

$$J(\theta_t) + \frac{\sqrt{2}(1-\omega)R_{\text{max}}}{(1-\gamma)^2} \sqrt{H-\kappa} \geq J(\theta_{\text{mix}}) \geq J(\theta_t) - \frac{\sqrt{2}(1-\omega)R_{\text{max}}}{(1-\gamma)^2} \sqrt{H-\kappa} \quad (21)$$

where $H = \mathbb{E}_{s \sim d_{\pi_{\text{mix}}}^t} \mathcal{H}(\pi^t(\cdot|s))$ represents the average entropy of the teacher policy, κ is a small error term, R_{max} represents the maximum reward value, and ω is the intervention rate determined by the switch function.

Appendix A presents a detailed derivation of Theorem 3, which demonstrates that, via the switch function, the student can effectively improve the upper bound of performance through teacher interventions while maintaining a guaranteed lower bound. Furthermore, the student’s performance is strongly influenced by the quality of the teacher.

Simultaneously, to illustrate the improvement in safety performance of S2CD resulting from teacher policy intervention, we introduce Theorem 4 to demonstrate that the expected cumulative reward obtained by policy π^{mix} is guaranteed to be greater than or equal to the expected cumulative reward obtained by policy π^t , as expressed by:

Theorem 4. *The expected cumulative reward obtained by learning from π^{mix} is guaranteed to be greater than or equal to the expected cumulative reward obtained by π^t :*

$$\mathbb{E}_{\pi^{\text{mix}}} \left[\sum_{t=0}^H \gamma^t r(s_t, a_t) \right] \geq \mathbb{E}_{\pi^t} \left[\sum_{t=0}^H \gamma^t r(s_t, a_t) \right] \quad (22)$$

Appendix B presents a detailed derivation of Theorem 4, where Eq. 22 shows that the S2CD framework can ensure enhanced driving safety performance through the teacher’s guidance.

Model training with dual-source data When action a_t is executed, the environment provides feedback, such as the return, to the student agent for updating the neural network. At this point, the student agent has two complete sets of data available for training and optimizing the policy π^s : (s'_t, a_t, r_t) consists of on-policy data collected by executing action a_t in the current state s'_t and receiving environmental feedback r_t , while the other set (s'_t, a_t^t, r_t^t) is off-policy data provided by the teacher module, where action a_t^t and the return r_t^t are predicted based on state s_t . Due to the additional data provided by the teacher model, the S2CD framework achieves significantly higher sample efficiency. For the two distinct data sources from the teacher and student, the teacher’s guidance is particularly crucial, especially during the early stages of training. Therefore, to further enhance the learning efficiency of the algorithm, we applied the ACPPO algorithm proposed in Section 3.2 to optimize and update the neural network. ACPPO improves learning efficiency by loosening the update magnitude for significant samples while tightening it for less important ones.

KL divergence constraint In addition, to enable the student policy to quickly approximate the distribution of the teacher policy, we adopted a behavior cloning mechanism. The KL divergence between the teacher’s and student’s policies is used as a constraint in the algorithm, and the objective function is reformulated as an unconstrained optimization problem using the Lagrangian method. The constraint function is as follows:

$$C_t^{KL} = D_{KL}(\pi^t(\cdot|s_t) || (\pi^s(\cdot|s'_t))) \quad (23)$$

So the objective function can be defined as follows:

$$L^{ACLI P'}(\theta) = \begin{cases} \mathbb{E}_{\pi_\theta} [\min (r_t(\theta) A^{\pi_\theta}(s, a), \text{clip}(r_t(\theta), 1 - (\epsilon + \epsilon'), 1 + (\epsilon - \epsilon')) A^{\pi_\theta}(s, a)) - \xi C_t^{KL}], & \text{if } a_t = a_t^s \\ \mathbb{E}_{\pi_\theta} [\min (r_t(\theta) A^{\pi_\theta}(s, a), \text{clip}(r_t(\theta), 1 - (\epsilon - \epsilon'), 1 + (\epsilon + \epsilon')) A^{\pi_\theta}(s, a)) - \xi C_t^{KL}], & \text{if } a_t = a_t^t \end{cases} \quad (24)$$

where ξ represents the Lagrange multiplier for C_t^{KL} , and its initial value is provided in the [Table 1](#).

Intervention decay The teacher's intervention can significantly accelerate the student's learning process and prevent dangerous actions, thereby greatly enhancing the student's model performance, especially during the early stages of training. However, since the teacher's policy has an upper performance limit, over-reliance on the teacher's guidance can constrain the student's ultimate performance. To address this issue, we introduced a weaning mechanism that gradually reduces the teacher's intervention in the student during the mid-to-late stages of training, thereby mitigating the influence of the teacher's policy. This allows the S2CD framework to effectively balance teacher guidance with student exploration, ultimately achieving superior performance compared to a single policy. The weaning mechanism consists of two main components:

- We introduce the decay factor τ , which gradually increases the tolerance of the teacher's policy toward the student. Specifically, the tolerance increases by $1 - \tau$, leading to a progressive reduction in the intervention probability ω of the teacher's actions, ultimately decreasing it to 0.
- Secondly, as the teacher's intervention probability progressively decreases, we utilize τ to gradually reduce both the adaptive factor ϵ' and the constraint function C_t^{KL} , thereby diminishing the teacher's influence on the student.

Thus, the final objective function of the S2CD framework is defined as follows:

$$L^{S2CD}(\theta) = \begin{cases} \mathbb{E}_{\pi_\theta} [\min (r_t(\theta) A^{\pi_\theta}(s, a), \text{clip}(r_t(\theta), 1 - (\epsilon + \tau\epsilon'), 1 + (\epsilon - \tau\epsilon')) A^{\pi_\theta}(s, a)) - \tau\xi C_t^{KL}], & \text{if } a_t = a_t^s \\ \mathbb{E}_{\pi_\theta} [\min (r_t(\theta) A^{\pi_\theta}(s, a), \text{clip}(r_t(\theta), 1 - (\epsilon - \tau\epsilon'), 1 + (\epsilon + \tau\epsilon')) A^{\pi_\theta}(s, a)) - \tau\xi C_t^{KL}], & \text{if } a_t = a_t^t \end{cases} \quad (25)$$

According to the decay coefficient, in the early stages of training, as much prior knowledge as possible is provided to guide ACPPO learning. In the middle and late stages of training, it becomes necessary to gradually reduce the influence of the teacher policy on the student. And as decay coefficient gradually decreases, the objective function $L^{S2CD}(\theta)$ will regress to the objective function of the regular PPO algorithm, as shown in [Eq. 11](#). We update the ACPPO agent by maximizing $L^{S2CD}(\theta)$.

The process of the S2CD decision-making framework is outlined in [Algorithm 2](#), and all parameters are listed in [Table 1](#).

3.3.3 Low-level Layer

In our proposed S2CD decision-making framework, we have designed a hierarchical architecture to facilitate the smooth driving of autonomous vehicles in complex and dynamic traffic environments. Initially, the high-level decision-making layer generates either a follow or a lane-change command based on the state s'_t . Subsequently, the low-level layer executes path planning and controls the vehicle's driving trajectory and speed in accordance with the high-level commands. As this paper primarily concentrates on high-level decision-making algorithms, we have opted for classic and reliable algorithms for the low-level layer.

Path planning layer In the path planning layer, we employ cubic spline functions to plan the vehicle's driving path. The centerline points of the driving path are defined as $(x_0, y_0), (x_1, y_1), \dots, (x_n, y_n)$. Each S_i , representing the segment along the interpolated centerline, is bounded by (x_i, y_i) and (x_{i+1}, y_{i+1}) . The cubic spline function is defined as follows:

$$y_i(x) = a_i + b_i(x - x_i) + c_i(x - x_i)^2 + d_i(x - x_i)^3 \quad (26)$$

where parameters a_i, b_i, c_i , and d_i can be solved using the methods outlined in [Paper Jiang et al. \(2020\)](#).

The global trajectory is determined by Carla's navigation points. When the high-level command is a lane change, we set the lateral position of the next navigation point on the centerline of the target lane, maintaining a longitudinal distance of 10 m from the current position. Subsequently, cubic spline interpolation is employed for local path planning along this segment of the trajectory.

Algorithm 2: S2CD Decision-Making Framework

Input: Complex Environment State s_t , Teacher Action a_t^t , Predicted Return Value r_t^t , Q-value Q_t^t
Output: Ego Vehicle Action a_t

```

1 Randomly initialize Actor network  $NN_1$  and Critic network  $NN_2$  with weights  $\theta_1$  and  $\theta_2$ 
2 Copy Actor and Critic networks to Actor and Critic target networks respectively:
    $NN'_1 \leftarrow NN_1, NN'_2 \leftarrow NN_2, \theta'_1 \leftarrow \theta_1, \theta'_2 \leftarrow \theta_2$ 
3 for  $n = 1 : N_{total}$  do
4   for  $t = 1 : T_{epoch}$  do
5     Get action from teacher policy  $\pi^t$ :  $a_t^t \leftarrow \pi^t(\cdot | s_t)$ 
6     Add  $a_t^t$  to  $s_t$ :  $s'_t \leftarrow s_t$ 
7     Get action from student policy  $\pi^s$ :  $a_t^s \leftarrow \pi^s(\cdot | s'_t)$ 
8     Compute advantage estimates  $A^{\pi_\theta}$ 
9     Predict Q-values of  $a_t^s$  and  $a_t^t$ :  $Q_t^s, Q_t^t \leftarrow$  Q-Value network
10    if  $Q_t^t - Q_t^s > (1 - \tau)\varepsilon$  then
11      | Choose action under the guidance of teacher model:  $a_t \leftarrow a_t^t$ 
12    else
13      | Choose action based on Actor network:  $a_t \leftarrow a_t^s$ 
14    end
15    Adopt  $a_t$  and collect  $(s'_t, a_t, r_t, s'_{t+1})$  into replay buffer  $B$ 
16    Predict return value of  $a_t^t$ :  $r_t^t \leftarrow$  Return network
17    Collect  $(s'_t, a_t^t, r_t^t, s'_{t+1})$  into replay buffer  $B$ 
18    Compute Kullback-Leibler divergence of teacher and student policies:  $D_{KL}(\pi^t(\cdot | s_t) || \pi^s(\cdot | s'_t))$ 
19    Compute adaptive clipping factor  $\epsilon'$ 
20    Update decay coefficient  $\tau$ 
21  end
22  Update Actor network  $NN_1$  and Critic network  $NN_2$  using  $B$ ,  $A^{\pi_\theta}$  and  $D_{KL}$  by maximizing  $L^{S2CD}(\theta)$ :
    $\theta_1^{new}, \theta_1'^{new}, \theta_2^{new}, \theta_2'^{new} \leftarrow \theta_1, \theta_1', \theta_2, \theta_2'$ 
23 end

```

Table 2: Parameters of IDM model

Parameters	Value
Desired speed v_0	25 m/s
Desired time gap T	0.6 s
Safety gap s_0	2.0 m
Acceleration exponent ζ	4
Maximal acceleration a	$2m/s^2$
Comfortable deceleration b	$2m/s^2$

Table 3: Parameters of PID controller

Parameters	Value
Proportional Gain of lateral control K_P	0.75
Derivative Gain of lateral control K_D	0.01
Integral Gain of lateral control K_I	0.2
Proportional Gain of longitudinal control K'_P	0.37
Derivative Gain of longitudinal control K'_D	0.012
Integral Gain of longitudinal control K'_I	0.016

Control layer In this paper, we exclusively focus on lateral decision-making, which encompasses lane changes as well as following behavior. To maintain simplicity and prevent the over-conservative behavior of the agent, acceleration and speed are controlled by the Intelligent Driver Model (IDM) (Treiber et al., 2000). The target acceleration \dot{v}_e of the ego vehicle can be calculated using Eq. 27:

$$\dot{v}_e = a \left[1 - \left(\frac{v_e}{v_0} \right)^\zeta - \left(\frac{\max \left(s_0 + v_e T + \frac{v_e(v_e - v_1)}{2\sqrt{ab}}, 0 \right)}{s} \right)^2 \right] \quad (27)$$

where v_e is the speed of the ego vehicle, v_1 is the speed of the front vehicle, and other parameters of IDM are detailed in Table 2. With the target acceleration and current speed, the next moment's target speed can be determined.

Once the reference driving path and target speed are obtained, the control layer utilizes the PID algorithm to calculate the values for the vehicle's throttle, brake, and steering angle, employing two sets of PID parameters separately for lateral control and longitudinal control. All PID parameters are shown in Table 3.

4 Implementation

This section details the implementation of our simulation experiments. First, we compare the differences between the Highway-Env and Carla simulation environments. Then, we provide a detailed description of the medium-density highway lane-change scenario. Next, we model the driving scenario as a Markov Decision Process (MDP). Finally, we specify the parameter settings used in the simulation.

4.1 Highway-Env and Carla Simulation Environments

Highway-Env and Carla are widely used simulation environments in autonomous driving research. However, they differ significantly in terms of the complexity of decision-making processes, the level of control detail, and computational resource requirements. Highway-Env represents the environment as a simplified 2-dimensional plane and reduces vehicle actions to discrete choices, such as accelerating, decelerating, and lane changing. Consequently, the decision-making process in this environment is relatively straightforward, typically requiring only tens to hundreds of simulation steps to complete a task. Because of the simplified environment, the simulation avoids complex perception data processing. Additionally, the vehicle dynamics model is highly abstracted, ignoring real-world physical characteristics. As a result, Highway-Env is extremely resource-efficient, achieving simulation speeds of hundreds or even thousands of iterations per second on standard computing devices. This makes it ideal for large-scale RL training and strategy validation.

In contrast, Carla provides a high-fidelity 3-dimensional simulation environment that can model complex traffic scenarios and support the processing of various sensor data (e.g., cameras, LiDAR), along with continuous vehicle control. The complexity of the environment and vehicle dynamics necessitates that the decision-making process consider multi-dimensional continuous control variables, such as steering angle, throttle, and brake force. A typical driving task in Carla may require thousands to tens of thousands of simulation steps to complete. Additionally, Carla requires higher simulation precision, involving high-dimensional sensor data processing and detailed physical simulations, which typically necessitates high-performance computing devices support. Consequently, Carla's simulation speed is relatively slow, achieving only a few to tens of simulation steps per second. This makes Carla more suitable for testing and validating autonomous driving systems in complex environments, especially when real-world perception, planning, and control challenges are the focus.

In summary, Highway-Env is well-suited for the rapid validation of simple decision-making processes, particularly in RL strategy research, due to its simplified environment and lower computational requirements. In contrast, Carla provides a more realistic testing platform for developing and validating complex autonomous driving systems. The differences between the two environments are not only reflected in the simplification of environment representation and action space but also in the significant disparity in the number of decision steps required and the computational resources consumed by the simulations.

4.2 Scenarios Specification

Medium traffic density on highways is characterized by approximately 15 vehicles per lane per kilometer, with vehicle spacing ranging from 50 m to 90 m (Gold et al., 2016). This density strikes a balance by avoiding congested traffic, which hinders lane changes, and low-density traffic, where lane changes become unnecessary. Consequently, it serves as a typical representation of most lane-change scenarios. We employ the medium-density traffic scenario as a comprehensive platform to train and evaluate the performance of the S2CD lane-change decision-making framework. Fig. 3 illustrates the scenario's performance in the Highway-Env and Carla simulation environments, where the ego vehicle navigates a 3-lane highway and executes lane changes while surrounded by other vehicles. Consistent with driving knowledge and applicable traffic regulations, the ego vehicle must consider the positions and movements of vehicles ahead, as well as those to its front-left, rear-left, front-right, and rear-right, during lane-change decision-making. Therefore, the real-time states of these surrounding vehicles (such as speed and distance) are integrated into the model's input.

In the experiment, both the ego vehicle and surrounding vehicles start with an initial speed of 0 m/s, while the ego vehicle's maximum speed is limited to 25 m/s. To more accurately replicate real-world driving conditions, the target speeds of the surrounding vehicles are randomly selected within the range of 15 to 25 m/s. Poor lane-change decisions may result in collisions between the ego vehicle, other vehicles, or road boundaries. An episode is considered complete if the ego vehicle successfully drives 1 km without any collisions. If a collision occurs, the episode is marked as failed, and the environment is reset for the next episode.

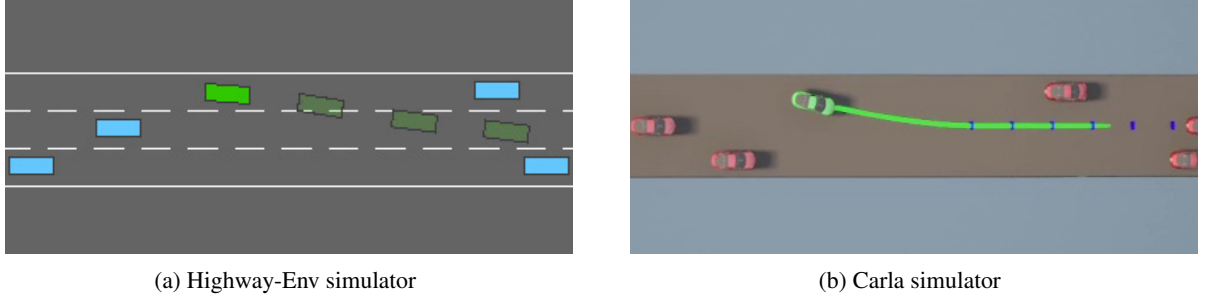


Figure 3: Medium-density traffic scenario with 3-lanes

4.3 Scenario Modeling

Next, we define the state space, action space, and return function, thereby modeling the driving scenario as a Markov Decision Process (MDP).

4.3.1 State

The state s_t encompasses observations of the ego vehicle, including driving information features from both the ego vehicle and surrounding vehicles. As described in Section 4.2, at time t , s_t is defined as follows:

$$s_t = (v_{e,t}, \{v_{i,t}, d_{i,t}\}) \quad (28)$$

where v_e is the speed of the ego vehicle. The speeds of surrounding vehicles and their longitudinal positions relative to the ego vehicle are represented as $\{v_i, d_i\}$, where $i = (1, 2, 3, 4, 5)$ corresponds to the front vehicle, left front vehicle, left rear vehicle, right front vehicle, and right rear vehicle, respectively. To obtain more accurate state features, we make the following assumptions:

1. When the ego vehicle is driving in the nearside lane, one side of the ego vehicle will have no surrounding vehicles. In this case, $\{v_i, d_i\}$ for vehicles on that side will be set to $\{0 \text{ m/s}, 100 \text{ m}\}$.
2. If the ego vehicle is not driving in the nearside lane and there are no other vehicles in a side lane, or if vehicles in a side lane are outside of the perception range, the $\{v_i, d_i\}$ for vehicles on that side will be set to $\{0 \text{ m/s}, 50 \text{ m}\}$.

4.3.2 Action

In this paper, the decision-making layer provides only discrete meta-actions, which serve as high-level commands for the path planning and control layer. Consequently, the high-level action a_t of the ego vehicle at time t can be defined as follows:

$$a_t = (a_1, a_2, a_3) \quad (29)$$

where a_1, a_2 , and a_3 represent Follow, Left Lane Change, and Right Lane Change, respectively.

4.3.3 Return

In the highway lane-change scenario, the primary objective of autonomous vehicles is to achieve high-speed driving while avoiding collisions. Therefore, to guide the ego vehicle in increasing speed while maintaining a high level of safety, the return function in this paper is composed of two parts:

1. **Efficiency Reward:** The maximum speed of the ego vehicle is set to 25 m/s. To encourage the ego vehicle to accelerate from 0 m/s to higher speeds, we employ an efficiency reward function, defined as follows:

$$R_e = \begin{cases} 0, & \text{if } 0 < v_e < 12.5 \text{ m/s} \\ \alpha_1 \left(\frac{v_e}{12.5} - 1 \right), & \text{if } 12.5 \text{ m/s} < v_e < 25 \text{ m/s} \\ \alpha_1, & \text{otherwise} \end{cases} \quad (30)$$

where $\alpha_1 > 0$ represents the weight coefficient used to adjust the importance of efficiency reward in the strategy.

Table 4: Parameters of Highway-Env simulation

Parameters	Value
Lanes count	3
Lane width	3.75m
Vehicle model	Kinematic
Simulation frequency	10Hz
Policy frequency	2Hz
Auto lane change for other vehicle	True
Speed limit	25m/s

Table 5: Parameters of Carla simulation

Parameters	Value
Lanes count	3
Lane width	3.75m
Vehicle model	Dynamic
Synchronous mode	True
Simulation time step	0.05s
Auto lane change for other vehicle	True
Speed limit	25m/s

2. **Safety Cost:** The safety cost depends on the safe distance d_{safe} , which represents the longitudinal distance between the ego vehicle and the vehicles in front or rear, as well as whether a collision occurs. The safety cost function can be defined as follows:

$$C_s = \begin{cases} \alpha_2, & \text{if } 0 < d_{safe} < 5 \text{ m} \\ \alpha_2 \left(1 - \frac{d_{safe} - 5}{5}\right), & \text{if } 5 \text{ m} < d_{safe} < 10 \text{ m} \\ 1, & \text{if collision} \\ 0, & \text{otherwise} \end{cases} \quad (31)$$

where $\alpha_2 > 0$ represents the weight coefficient used to adjust the importance of safety cost in the strategy.

The weight coefficients α_1 and α_2 are adjusted based on the results of multiple experiments, and their specific values are provided in Table 1. The final return function R is presented in Eq. 32:

$$R = R_e - C_s \quad (32)$$

4.4 Simulation Settings

All experiments in this paper were conducted on a computer equipped with an Intel i5-13600KF CPU, an NVIDIA GeForce RTX 4090 GPU, and 32GB of RAM. The experiments involved two simulation environments, Highway-Env and Carla, with their respective runtime parameters listed in Table 4 and Table 5. As this paper focuses on decision-making methods, we simplified the perception module by assuming that the ego vehicle can directly obtain accurate information (e.g., speed, distance) about other vehicles within a 50 m radius. To demonstrate the algorithm's generalization ability, different random seeds were employed each time the environment was reset. In the Carla simulation environment, all vehicles except the ego vehicle were managed by the simulator's traffic manager, which controls behaviors such as car-following and lane-change. In the Highway-Env simulation environment, other vehicles were managed using simple decision-making algorithms (e.g., IDM, MOBIL) and control algorithms (e.g., proportional controllers).

Since Highway-Env is a simplified simulation environment, while Carla is a high-fidelity simulation environment, simulating the same 1 km drive requires nearly 1,500 steps in Carla, compared to fewer than 150 steps in Highway-Env. Specifically, when the ego vehicle makes a lane-change decision, the policy frequency in Highway-Env is set to 2, allowing the lane-change process to be completed in only 2 steps. This simplification facilitates the training of effective teacher models using RL algorithms. In contrast, the lane-change process in Carla requires 10 to 20 steps. Consequently, obtaining an effective lane-change decision model using standard RL algorithms in Carla is challenging.

5 Simulation Result

We conducted performance testing and comparisons of the proposed S2CD against other state-of-the-art (SOTA) methods in a highway lane-change scenario:

DQN (Deep Q-Network (Mnih, 2013), Value-based RL): DQN integrates deep learning with Q-learning by using a neural network to approximate Q-values, significantly improving performance in high-dimensional discrete state tasks.

PPO (Proximal Policy Optimization (Schulman et al., 2017), On-Policy RL): PPO employs clipped policy updates to ensure stability and efficiency in optimization, widely applied in both continuous and discrete control tasks.

SAC (Soft Actor-Critic (Haarnoja et al., 2018), Off-Policy RL): SAC maximizes policy entropy to encourage exploration, significantly enhancing sample efficiency and performance in continuous action spaces.

PPO-Lag (PPO with Lagrangian Multipliers (Stooke et al., 2020), Safe RL): PPO-Lag extends PPO by introducing Lagrangian multipliers to handle constrained optimization, ensuring policy updates adhere to constraints while optimizing the objective.

SAC-Lag (SAC with Lagrangian Multipliers (Ha et al., 2021), Safe RL): SAC-Lag extends SAC by incorporating Lagrangian multipliers to balance policy entropy with constraint satisfaction, making it suitable for constrained RL.

TS2C (Teacher-Student Shared Control (Xue et al., 2023), TSF): TS2C is a student-teacher framework where a pre-trained teacher agent guides the student agent by intervening and providing online demonstrations based on trajectory-based value estimation, and we re-implemented this algorithm using PPO as the base method.

SOAR-ACPPO (SOAR Cognitive Architecture with Adaptive Clipping PPO (Zhou et al., 2024), TSF): SOAR-ACPPO is a hybrid decision-making framework based on the TSF, where the SOAR cognitive decision model, incorporating human driving knowledge, serves as the teacher to effectively guide the student agent, which is based on the ACPPO algorithm.

BC (Behavioral Cloning (Pomerleau, 1991), IL): BC is a supervised imitation learning algorithm that directly learns policies by mimicking expert actions from example data.

GAIL (Generative Adversarial Imitation Learning (Ho and Ermon, 2016), IL): GAIL combines the generative adversarial framework with imitation learning, using a discriminator to distinguish between expert and learner policies, guiding the learner towards expert-level performance.

CQL (Conservative Q-Learning (Kumar et al., 2020), Offline RL): CQL is an offline reinforcement learning algorithm that penalizes overestimation of Q-values, ensuring conservative policy updates, which is particularly effective when learning from static datasets.

In Safe RL algorithms, we introduce safety cost as constraints to regulate policy behavior, ensuring that the agent maximizes efficiency reward while adhering to safety constraints. The specific parameters of the baseline algorithms are provided in Appendix C. Our analysis compares two aspects: model training and evaluation.

- 1) **Model Training:** Each algorithm was trained 3 times, using different random seeds to capture their average performance. The model is tested every 5,000 steps during the training process, and the results are recorded to evaluate its training efficiency and performance.
- 2) **Model Evaluation:** Following training, each algorithm was evaluated 6 times with different random seeds to ensure an accurate assessment of average performance. These test results primarily evaluate the models' success rates in safely driving a target distance of 1 km without collisions, while also assessing traffic efficiency and driving safety throughout the process. Additionally, all models were evaluated in both high-density and low-density highway scenarios.

5.1 Model Training

Fig. 4 presents the test results of various algorithms during the model training process. The metrics presented include the return, safety cost, average speed from test episodes, as well as efficiency reward, safety cost, and collision counts generated from the agent's interactions with the environment every 5,000 steps. Notably, CQL, as an offline RL algorithm, does not depend on interactions with the environment for data collection during training. Therefore, CQL has been excluded from this comparison.

Throughout the training process of the algorithms, we primarily focus on the trends of key indicators, such as model performance and safety. Fig. 4a illustrates the test return curve as a function of training steps, clearly reflecting the overall performance of all algorithms. As the curve indicates, guided by the teacher model, S2CD benefits from higher sample efficiency and learning efficiency, enabling it to acquire more accurate knowledge in the early stages. This advantage allows it to cover longer distances without collisions, thereby achieving consistently high return values of approximately 240 from the outset. For the TS2C algorithm, excessive teacher intervention during the early stages leads to an imbalance between positive and negative samples, and the discrepancy between the policy distributions of the teacher and the student hampers the student's ability to optimize its policy, resulting in a lower Return. SOAR-ACPPO decides whether to intervene based on intervention probability, which prevents it from strictly following the teacher's guidance, consequently leading to a lower initial score. Nevertheless, SOAR-ACPPO's learning speed is significantly faster than that of other algorithms, except for S2CD. In contrast, other RL algorithms gradually optimize their policies through environmental interactions. However, due to limited early-stage knowledge, they experienced more frequent collisions during testing, resulting in significantly lower return values compared to S2CD. Furthermore, Fig. 4d demonstrates that the efficiency reward obtained by the S2CD and TS2C agents through interactions with the environment are considerably higher than those achieved by other algorithms, indicating that the teacher's intervention

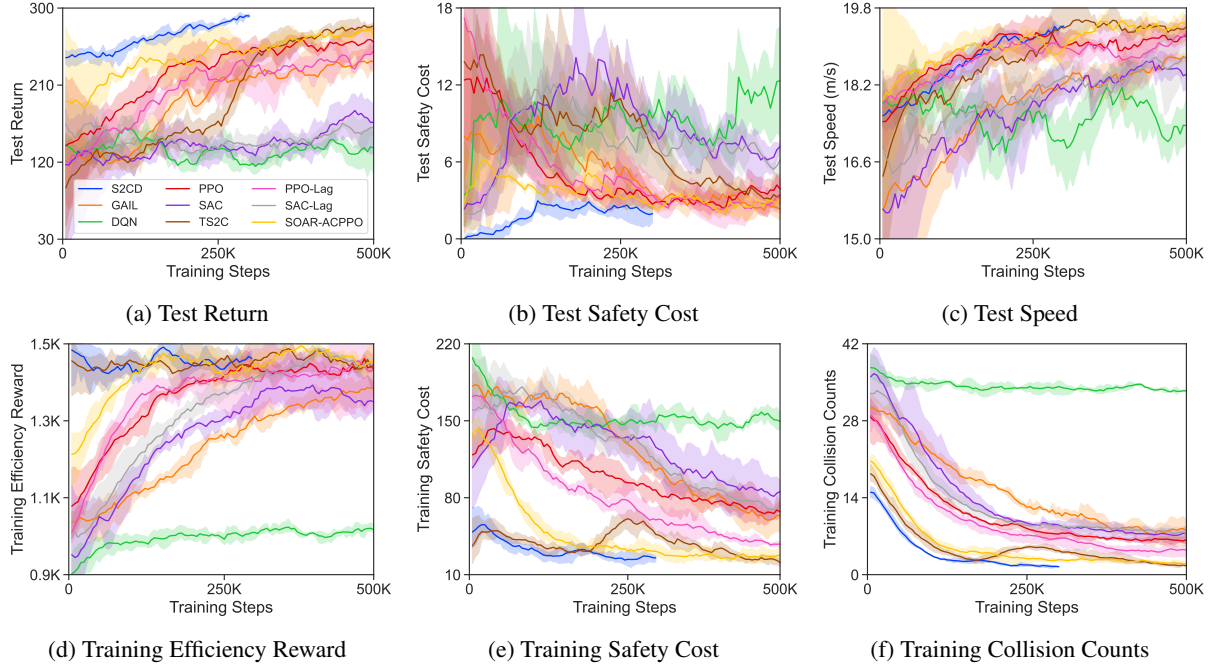


Figure 4: The training curves for all algorithms are presented. Each algorithm is trained with three different random seeds, accumulating a total of 500K training steps for each case, except for S2CD, which requires only 300K training steps. To ensure a comprehensive assessment of algorithm performance, two evaluation episodes are conducted for every 5,000 training steps. The average value of these two evaluation episodes is taken as the result.

effectively enhances the student’s ability to achieve high scores. Regarding safety, Fig. 4e illustrates the safety cost curves during the data collection period. Due to the teacher model’s intervention in correcting the student’s unsafe actions, S2CD and TS2C ensure that the ego vehicle maintains a safe distance from other vehicles whenever feasible. Consequently, this leads to their safety cost during the data collection period being significantly lower than that of other algorithms. However, as depicted in Fig. 4b, the TS2C algorithm demonstrates poor performance in terms of test safety cost, indicating the model’s inefficiency in learning. In contrast, S2CD consistently achieves the lowest test safety cost. Fig. 4f illustrates that during the early data collection phase, S2CD experienced the least number of collision events. Additionally, TS2C and SOAR-ACPPO, both benefiting from teacher guidance, also exhibited a similarly low collision probability, approximately half that of other algorithms. Therefore, even in the initial stages of training, when the policy is not yet fully optimized, the teacher’s guidance enables S2CD’s student agent to achieve performance and safety significantly superior to those of other algorithms.

During the mid-to-late stages of model training, as agents explore the environment more thoroughly, accumulate data, and update their policies, the performance of other algorithms, excluding DQN, begins to improve. Specifically, return, efficiency reward, and driving speed gradually increase, while safety cost and collision counts decrease. Notably, the PPO algorithm and its derivatives: S2CD, TS2C, SOAR-ACPPO, PPO-Lag, and GAIL, demonstrate significantly faster performance improvements, whereas SAC and its derivative SAC-Lag learn at a slower pace. This is because PPO-based algorithms limit the magnitude of policy updates, preventing substantial performance degradation in each iteration and ensuring that the policies steadily progress toward better solutions until convergence. Among these, TSF-based algorithms (S2CD, TS2C, SOAR-ACPPO) demonstrated relatively superior final performance. In contrast, because SAC-based algorithms are inherently designed for continuous action tasks, achieving satisfactory training results for the discrete action tasks in this study is challenging. In terms of training efficiency, S2CD’s enhancements in sampling and learning mechanisms result in a noticeably faster convergence speed, achieving a return greater than 290 with only 300K steps. This sharply contrasts with other algorithms, which require 500K steps to achieve convergence while exhibiting inferior performance. Although the safety cost of S2CD experiences a slight increase during the intermediate stages, it subsequently declines in the later stages and consistently remains lower than that of other algorithms. Notably, S2CD experiences significantly fewer collisions than other algorithms during the entire training process, with only approximately 2 collisions occurring every 5,000 training steps in the later stage. This indicates that S2CD demonstrates exceptionally high safety performance during the training process, markedly outperforming other algorithms.

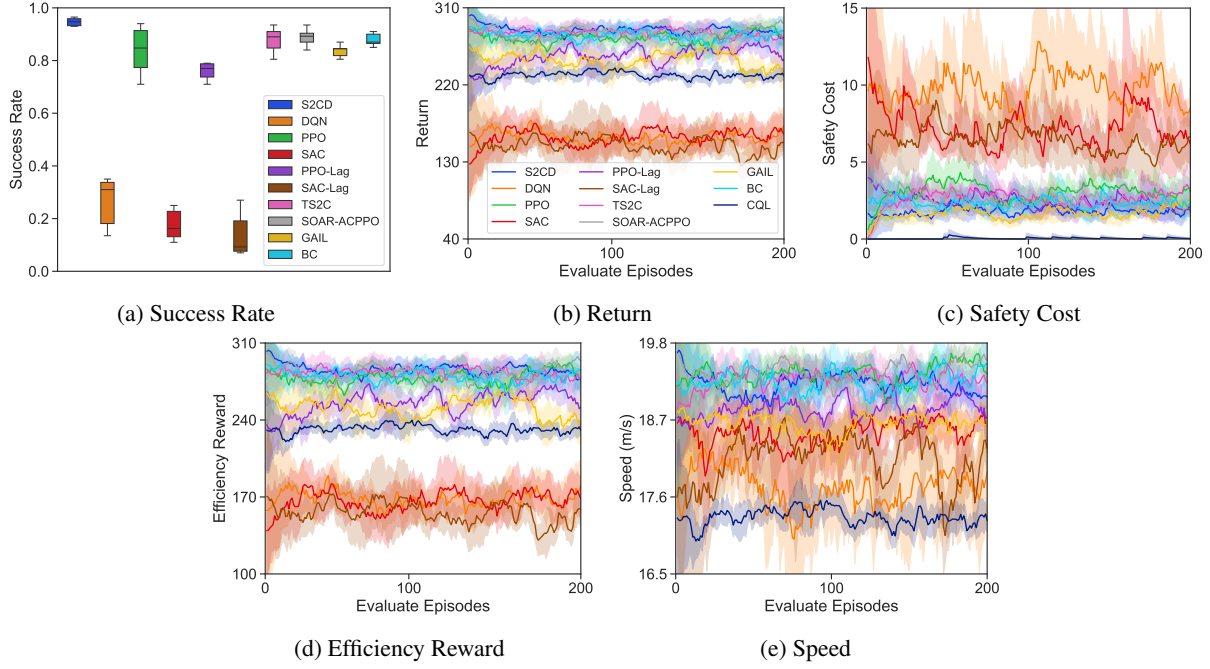


Figure 5: The curves of model evaluation for all algorithms. Each model trained with varying random seeds is evaluated twice, and each algorithm undergoes six evaluation runs, with each evaluation consisting of 200 episodes.

Table 6: The performance of all algorithms in the medium-density traffic scenario

Category	Method	Training Steps	Episodic Return	Episodic Reward	Episodic Cost	Episodic Speed (m/s)	Success Rate (%)
Value-Based RL	DQN	500K	159.85	169.60	9.75	17.74	26.50
On-Policy RL	PPO	500K	274.82	278.00	3.18	19.36	83.83
Off-Policy RL	SAC	500K	160.48	167.50	7.02	18.51	17.58
Safe RL	PPO-Lag	500K	254.29	256.68	2.39	18.85	76.00
	SAC-Lag	500K	148.80	155.28	6.48	18.17	13.67
TSF	TS2C	500K	280.24	283.05	2.80	19.30	87.83
	SOAR-ACPPO	500K	280.56	283.08	2.52	19.30	88.83
IL	GAIL	500K	248.17	249.90	1.73	18.65	83.67
	BC	/	277.53	279.87	2.35	19.27	87.90
Offline RL	CQL	/	231.47	231.51	/	17.31	/
Ours	S2CD	300K	283.14	284.96	1.82	19.19	94.67

Therefore, among conventional RL algorithms, PPO-based algorithms exhibit excellent performance during model training, while TSF-based algorithms more efficiently acquire superior strategies under teacher guidance. In particular, the proposed S2CD algorithm exhibited the best overall performance during both the training and testing phases.

5.2 Model Evaluation

After completing the training, we conducted a final performance evaluation of all models, as illustrated in Fig. 5 and presented in Table 6. It is worth noting that the offline RL algorithm CQL was trained using data collected online by the SAC algorithm. However, due to the poor performance of the SAC algorithm, CQL generated actions that consistently remained in "follow" mode even after training, failing to perform any lane-change actions. Therefore, we exclude its performance from further comparisons.

The results indicate that PPO-based algorithms significantly outperform both SAC-based algorithms and DQN, especially TSF-based algorithms, consistent with their performance during the training phase. Notably, S2CD demonstrates superior performance in two key metrics: success rate and return value, achieving a success rate of 94.67% and a

Table 7: The performance of all algorithms in the high-density traffic scenario

Method	Episodic Return	Episodic Reward	Episodic Cost	Episodic Speed (m/s)	Success Rate (%)
DQN	46.48	66.32	19.84	14.12	18.83
PPO	141.02	144.44	3.42	15.11	92.83
SAC	58.28	76.93	18.65	14.99	18.00
PPO-Lag	127.93	134.56	6.63	15.10	79.17
SAC-Lag	62.78	71.55	8.77	14.83	13.50
TS2C	141.30	142.04	0.75	15.06	93.00
SOAR-ACPPO	142.89	146.37	3.47	15.11	94.25
GAIL	120.23	123.86	3.63	15.07	75.00
BC	141.70	142.32	0.63	14.99	93.75
CQL	140.12	140.12	/	14.88	/
S2CD	143.88	144.66	0.77	15.02	96.83

return value of 283.14. Although S2CD’s safety cost (1.82) and speed (19.19 m/s) are not the highest values, they are very close to the best values of 1.73 and 19.36 m/s, respectively. This slight discrepancy may be attributed to the fewer training steps undertaken by S2CD. It is important to note that, for IL algorithms, an expert policy must first be trained using PPO. This expert policy is subsequently used to collect a substantial amount of high-quality data for training the GAIL and BC models. Consequently, although GAIL and BC achieve performance levels close to those of S2CD, their training processes are more complex and time-consuming. In contrast, the PPO algorithm is not influenced by other policies, exploring the environment entirely autonomously. Despite its relatively low success rate and safety performance, PPO achieves the highest driving speed of 19.36 m/s by prioritizing higher efficiency reward. Both TS2C and SOAR-ACPPO not only account for the role of teacher guidance but also ensure that the student agent can freely explore the environment in the later stages by reducing the intervention probability. Consequently, they achieved higher driving speeds (19.30 m/s and 19.30 m/s) and lower safety cost (2.80 and 2.52). Their return values, reaching 280, are second only to the highest-performing S2CD. As shown in Fig. 5a, S2CD maintained stable performance due to the effective guidance of the teacher, achieving a success rate variance of only 3.5% across 6 evaluations, which is significantly lower than that of the PPO algorithm alone. Moreover, TS2C and SOAR-ACPPO also achieved exceptionally high success rates (87.83% and 88.83%), indicating that teacher guidance not only enhances the performance potential of the student models but also improves their safety thresholds. The performance of the SAC-based and DQN algorithms remained poor, consistent with their training phase results, with success rates not exceeding 30% and return value below 200, highlighting a significant gap compared to the PPO-based algorithms.

To validate the generalizability and superiority of the S2CD framework, we evaluated the performance of all compared algorithms in both high-density and low-density traffic scenarios. In the high-density traffic scenario, vehicle spacing was randomly set within a range of 20 m to 50 m, resulting in an average vehicle density of approximately 29 vehicles per kilometer per lane. In contrast, in the low-density traffic scenario, vehicle spacing was randomly set within a range of 90 m to 120 m, resulting in an average vehicle density of approximately 9 vehicles per kilometer per lane. The average evaluation results for these scenarios are presented in Table 7 and Table 8, respectively. As shown in Table 7, in the high-density traffic scenario, the reduced vehicle spacing increases the complexity of the environment, further degrading the performance of the already underperforming DQN, SAC-Lag and GAIL algorithms. However, as lane-change opportunities become more limited, the frequency of lane-change by the ego vehicle significantly dropped, resulting in a reduced probability of collisions and, consequently, an improvement in the performance of other algorithms. S2CD continues to demonstrate the highest success rate (96.83%) and return value (143.88), while its safety cost (0.77) and speed (15.02 m/s) are also very close to the best values of 0.63 and 15.11 m/s. As shown in Table 8, in the low-density traffic scenario, the sparsity of traffic flow reduces the necessity for frequent lane-change to increase speed, thereby decreasing the probability of collisions and improving the safety performance and driving speed of all algorithms. S2CD achieved the highest success rate (98.75%) and return value (341.01), while also demonstrating the lowest safety cost (0.51). Additionally, its driving speed (21.32 m/s) is close to the highest speed achieved by the PPO algorithm, which is 21.68 m/s. Similarly, the overall performance of TSF-based TS2C and SOAR-ACPPO ranks second only to S2CD, outperforming other algorithms in both high-density and low-density traffic scenarios. This finding aligns with the results in the medium-density traffic scenario, further validating the effectiveness of teacher guidance.

The preceding discussion emphasizes that our proposed S2CD framework effectively balances the benefits of teacher guidance with autonomous exploration, thereby establishing a driving strategy that integrates both training efficiency and safety. Importantly, S2CD demonstrates the most superior performance among all the compared algorithms.

Table 8: The performance of all algorithms in the low-density traffic scenario

Method	Episodic Return	Episodic Reward	Episodic Cost	Episodic Speed (m/s)	Success Rate (%)
DQN	274.54	278.86	4.32	20.55	57.67
PPO	339.63	341.11	1.48	21.68	90.00
SAC	274.75	278.91	4.15	20.71	52.50
PPO-Lag	328.58	330.52	1.94	21.18	90.50
SAC-Lag	261.22	267.44	6.21	20.75	44.33
TS2C	336.94	338.03	1.09	21.51	91.92
SOAR-ACPPO	339.95	340.82	0.87	21.52	95.00
GAIL	320.32	321.41	1.09	20.99	89.50
BC	340.60	341.57	0.97	21.46	91.67
CQL	274.77	274.80	/	18.78	/
S2CD	341.01	341.52	0.51	21.32	98.75

Table 9: Computational cost for different teacher models

Computational Cost	Training Steps	Training Processes	Time Spent (h)	GPU Memory Footprint (GB)	Memory Footprint (GB)	CPU Utilization (%)
Simple Teacher-High	400K	4	1.98	4.68	3.82	20.38
Simple Teacher-Low	200K	2	1.96	3.03	3.06	12.60
Complex Teacher	400K	2	9.58	10.60	8.74	67.18

5.3 Ablation Study

To assess the contributions of each component in the S2CD framework and validate its effectiveness, we conducted ablation experiments. By gradually removing or replacing specific modules within the framework, we observed variations in performance. The ablation study validated the framework’s design rationale and demonstrated the role that each module plays in enhancing performance.

5.3.1 The Impact of Different Teacher Quality

To explore the impact of guidance from teachers of varying quality on student performance, we trained a high-quality teacher model and a low-quality teacher model in a simple simulation environment (Highway-Env), as well as an additional teacher model in a complex simulation environment (Carla). These 3 teacher models were subsequently applied to the S2CD framework to guide the learning of the student agent.

Table 9 presents the computational costs associated with different teacher models, including training steps, number of processes, time spent, GPU memory footprint, memory footprint, and CPU utilization. In the Highway-Env environment, training a low-quality teacher model requires 200K steps, whereas achieving a high-quality teacher model can be accomplished by simply doubling the number of data collection processes. Although the training steps and CPU utilization approximately doubled, the increases in time spent, GPU memory footprint, and memory footprint were minimal, with the training time remaining almost unchanged. Therefore, in the Highway-Env environment, a high-quality teacher model can be obtained at minimal computational cost. In contrast, training for the same 400K steps in the Carla simulation environment required nearly 5 times the time spent compared to Highway-Env, with the GPU memory footprint, memory footprint, and CPU utilization more than doubling. This indicates that the cost of training teacher models in complex simulation environments is significantly greater than in simpler ones. The 3 trained teacher models were integrated into the S2CD framework to guide the student agent’s learning in the Carla environment, with the training and evaluation results presented in [Fig. 6](#) and [Table 10](#).

The results demonstrate that higher-quality teacher models enable the student to acquire more accurate knowledge, resulting in improved performance during the later stages of training and in the final evaluation. Specifically, the return, the probability of avoiding collisions and the task success rate during training were higher with the high-quality teacher compared to the low-quality teacher. This indicates that high-performance teachers can significantly enhance the safety and performance of the student’s training. Additionally, we implemented a weaning mechanism that gradually reduces the teacher’s influence on the student agent in the later stages, allowing the student to explore the environment more independently. This mechanism elevated the algorithm’s performance ceiling, enabling the student to ultimately

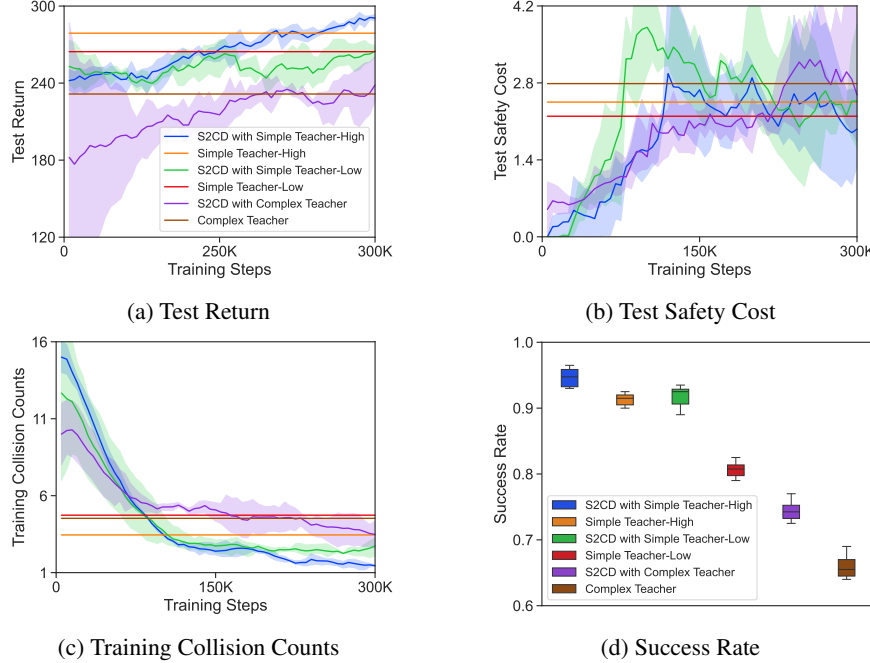


Figure 6: The training and evaluation processes involve different teacher models. 1. Model Training: Each algorithm is trained with three different random seeds, accumulating a total of 300K training steps for each case. Two evaluation episodes are conducted for every 5,000 training steps. The average value of these two evaluation episodes is taken as the result. During model training, we record the return value, safety cost, and collision counts. 2. Model Evaluation: Each model trained with varying random seeds is evaluated twice. Each algorithm undergoes six evaluation runs, with each evaluation consisting of 200 episodes. For model evaluation, we record the success rate.

Table 10: The performance of S2CD under the guidance of teachers at different levels

Experiment	Episodic Return	Episodic Reward	Episodic Cost	Episodic Speed (m/s)	Success Rate (%)
S2CD with Simple Teacher-High	283.14	284.96	1.82	19.19	94.67
Simple Teacher-High	281.21	283.69	2.48	19.28	91.30
S2CD with Simple Teacher-Low	272.19	274.32	2.13	18.98	91.75
Simple Teacher-Low	269.11	271.93	2.82	19.20	80.67
S2CD with Complex Teacher	243.59	245.57	1.98	18.87	74.42
Complex Teacher	238.64	241.03	2.39	19.07	66.00

surpass the teacher in key metrics such as return and success rates. Notably, although the teacher model trained in the Carla environment consumed significant computational resources, its performance was inferior to that of the low-quality teacher trained in the Highway-Env environment. The return and success rates were only 238.64 and 66.00%, respectively, significantly lower than those of the teachers trained in simpler environments. Furthermore, when guided by this teacher model, the student agent’s final performance was lower than that of the simple teacher. The return was approximately 40 lower, and the key metric, success rate, was about 20% lower. This demonstrates that training teacher models in a simple simulation environment not only saves substantial computational costs but also yields better performance, providing more effective guidance to the student agent.

5.3.2 Ablations of Guardian Mechanism

In this work, we introduce substantial enhancements to the traditional PPO algorithm. First, we utilized data from both the teacher and student models concurrently, effectively doubling the available training data and significantly improving sample efficiency. We then adapted the clipping factor of the algorithm based on the varying importance of these two data types, further enhancing the algorithm’s learning efficiency. Additionally, to ensure that the student policy rapidly approximates the teacher policy in the early stages of training, we employed the KL divergence between the two policies

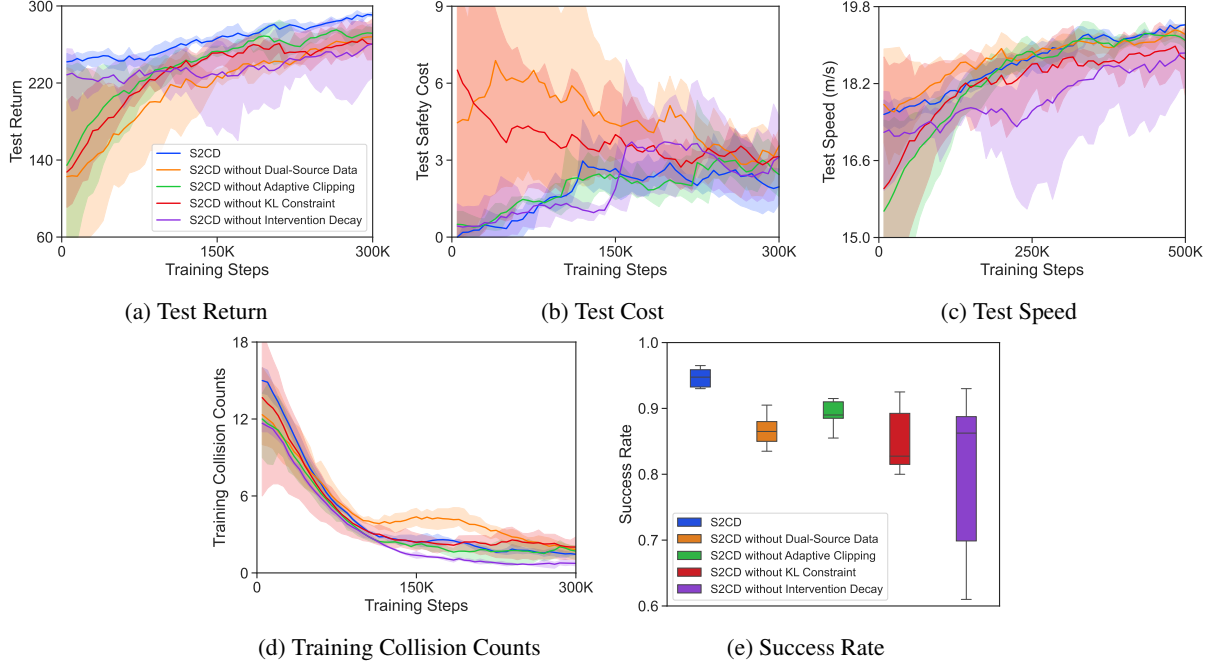


Figure 7: The training and evaluation processes of the ablation experiment. 1. Model Training: Each algorithm is trained with three different random seeds, accumulating a total of 300K training steps for each case. Two evaluation episodes are conducted for every 5,000 training steps, and the average value of these two episodes is taken as the result. During model training, we record the return value, safety cost, speed, and collision counts. 2. Model Evaluation: Each model trained with varying random seeds is evaluated twice, and each algorithm undergoes six evaluation runs, with each evaluation consisting of 200 episodes. For model evaluation, we record the success rate.

Table 11: The performance of S2CD in ablation experiments

Experiment	Episodic Return	Episodic Reward	Episodic Cost	Episodic Speed (m/s)	Success Rate (%)
S2CD	283.14	284.96	1.82	19.19	94.67
S2CD without Dual-Source Data	277.28	280.45	3.16	19.32	86.70
S2CD without Adaptive Clipping	274.24	276.68	2.45	19.08	89.10
S2CD without KL Constraint	262.09	265.94	3.85	18.63	85.08
S2CD without Intervention Decay	255.27	259.00	3.73	18.74	80.08

as a constraint of policy update. We subsequently applied the Lagrangian method to transform the optimization problem into an unconstrained format for policy updates. Finally, we implemented an annealing mechanism to preserve the agent’s exploratory capabilities, ensuring it can overcome the limitations of the teacher’s performance. By incorporating the 4 modules described above, our proposed algorithm not only significantly enhances learning efficiency but also improves the model’s performance and safety. To assess the contribution of each module to the overall performance, we conducted ablation experiments. In these experiments, we sequentially removed each module and analyzed the resulting performance changes to verify the necessity of each component. The training and evaluation results from the ablation experiments are presented in Fig. 7 and Table 11.

The experimental results indicate that the performance of the S2CD framework declines to some extent with the removal of any module. Specifically, when the teacher model’s intervention does not gradually diminish, the student performs well in the early stages of training and maintains a low collision rate throughout. However, in the later stages, the student struggles to break free from the influence of the teacher’s strategy. This not only leads to the student learning many of the teacher’s incorrect instructions but also hinders the student’s ability to explore freely and acquire more accurate knowledge. Ultimately, the return and success rates were only 255.27 and 80.08%, respectively, with a relatively low average speed of 18.74 m/s. This indicates that the gradual reduction of intervention is crucial for ensuring that the student agent ultimately surpasses the performance of the teacher model. As shown in Fig. 7a, the removal of

the "Dual-Source Data", "Adaptive Clipping", and "KL Constraint" modules significantly reduces the framework's performance in the early stages of training and negatively impacts the overall performance, leading to lower final outcomes for the model. The absence of these three modules diminishes the model's learning efficiency, thereby limiting the knowledge gained by the student agent. It is important to note that due to the imperfections in the teacher model's Return network and Q-Value network components, the use of additional training data and the inclusion of KL constraints carry the risk of the student learning incorrect information. This risk must be mitigated by gradually reducing the teacher's intervention.

The adaptive clipping module primarily accelerates the optimization process. Thus, after its removal, the model's final performance remains closest to that of the complete framework, with its success rate being only 5.57% lower than that of the full framework. The analysis above indicates that the "Dual-Source Data", "Adaptive Clipping", and "KL Constraint" modules primarily enhance the early-stage learning efficiency of the model, enabling the student to quickly absorb the knowledge provided by the teacher. In contrast, the intervention reduction module improves the performance ceiling of the student model by limiting excessive teacher intervention, aligning with the design goals of the S2CD framework.

6 Conclusion

This paper introduces a novel framework, S2CD, based on knowledge transfer techniques. The S2CD framework first trains a teacher model in a simplified simulation environment and then utilizes this model to guide the student agent in a more complex environment, enhancing the safety and efficiency of the training process. The paper also presents an innovative RL algorithm, ACPPO, which leverages samples generated by both teacher and student policies while dynamically adjusting the clipping factor based on sample importance, thereby improving learning efficiency. Moreover, the KL divergence between the teacher's and student's policies is incorporated as a constraint in model updates, solved using the Lagrangian method to enable the student agent to quickly adopt the teacher's policy. To further enhance the student agent's performance, a gradual weaning strategy reduces teacher intervention, ensuring that in the later stages of training, the student becomes more autonomous and explores optimal policies independently. Experimental results in highway lane-change scenarios demonstrate that compared to traditional RL, Safe RL, Offline RL, IL, and TSF algorithms, the S2CD framework significantly enhances both learning efficiency and model performance, while also reducing training costs. Most importantly, even with suboptimal teacher performance, the S2CD framework enhances safety during training. The framework is also applicable beyond varying simulation environments and offers a foundation for future knowledge transfer research between simulation and real-world environments.

The primary limitation of this study is that all experiments were conducted in simulated environments, without utilizing teacher models trained in simulation environments to guide student models in real-world conditions. Therefore, the next step in our research will involve real-world vehicle experiments to further validate the effectiveness and practicality of the proposed framework. Additionally, this study did not consider mixed traffic scenarios involving both autonomous and non-autonomous vehicles, which represents another crucial direction for future research to expand the applicability and coverage of the S2CD framework.

Acknowledgements

This work was supported by the National Natural Science Foundation of China (NSFC) under grant number 51975194.

References

- Akhauri, S., Zheng, L.Y., Lin, M.C., 2020. Enhanced transfer learning for autonomous driving with systematic accident simulation, in: 2020 IEEE/RSJ International Conference on Intelligent Robots and Systems (IROS), IEEE. pp. 5986–5993.
- Alvaro, P.K., Burnett, N.M., Kennedy, G.A., Min, W.Y.X., McMahon, M., Barnes, M., Jackson, M., Howard, M.E., 2018. Driver education: Enhancing knowledge of sleep, fatigue and risky behaviour to improve decision making in young drivers. *Accident Analysis & Prevention* 112, 77–83.
- Bae, S.H., Joo, S.H., Pyo, J.W., Yoon, J.S., Lee, K., Kuc, T.Y., 2020. Finite state machine based vehicle system for autonomous driving in urban environments, in: 2020 20th International Conference on Control, Automation and Systems (ICCAS), IEEE. pp. 1181–1186.
- Bengio, Y., Louradour, J., Collobert, R., Weston, J., 2009. Curriculum learning, in: Proceedings of the 26th annual international conference on machine learning, pp. 41–48.

Bianco-Vega, R., Hernández-Orallo, J., Ramírez-Quintana, M.J., 2005. Knowledge acquisition through machine learning: minimising expert's effort, in: Fourth International Conference on Machine Learning and Applications (ICMLA'05), IEEE. pp. 6–pp.

Bojarski, M., Del Testa, D., Dworakowski, D., Firner, B., Flepp, B., Goyal, P., Jackel, L.D., Monfort, M., Muller, U., Zhang, J., et al., 2016. End to end learning for self-driving cars. arXiv preprint arXiv:1604.07316 .

Buehler, M., Iagnemma, K., Singh, S., 2009. The DARPA urban challenge: autonomous vehicles in city traffic. volume 56. springer.

Cao, Z., Xu, S., Jiao, X., Peng, H., Yang, D., 2022. Trustworthy safety improvement for autonomous driving using reinforcement learning. *Transportation research part C: emerging technologies* 138, 103656.

Chen, S., Zhang, S., Shang, J., Chen, B., Zheng, N., 2017. Brain-inspired cognitive model with attention for self-driving cars. *IEEE Transactions on Cognitive and Developmental Systems* 11, 13–25.

Chow, Y., Nachum, O., Duenez-Guzman, E., Ghavamzadeh, M., 2018. A lyapunov-based approach to safe reinforcement learning. *Advances in neural information processing systems* 31.

Ferguson, D., Baker, C., Likhachev, M., Dolan, J., 2008. A reasoning framework for autonomous urban driving, in: 2008 IEEE Intelligent Vehicles Symposium, IEEE. pp. 775–780.

García, J., Fernández, F., 2015. A comprehensive survey on safe reinforcement learning. *Journal of Machine Learning Research* 16, 1437–1480.

Gold, C., Körber, M., Lechner, D., Bengler, K., 2016. Taking over control from highly automated vehicles in complex traffic situations: The role of traffic density. *Human factors* 58, 642–652.

Ha, S., Xu, P., Tan, Z., Levine, S., Tan, J., 2021. Learning to walk in the real world with minimal human effort, in: Conference on Robot Learning, PMLR. pp. 1110–1120.

Haarnoja, T., Zhou, A., Abbeel, P., Levine, S., 2018. Soft actor-critic: Off-policy maximum entropy deep reinforcement learning with a stochastic actor, in: International conference on machine learning, PMLR. pp. 1861–1870.

Hawke, J., Shen, R., Gurau, C., Sharma, S., Reda, D., Nikolov, N., Mazur, P., Micklethwaite, S., Griffiths, N., Shah, A., et al., 2020. Urban driving with conditional imitation learning, in: 2020 IEEE International Conference on Robotics and Automation (ICRA), IEEE. pp. 251–257.

Ho, J., Ermon, S., 2016. Generative adversarial imitation learning. *Advances in neural information processing systems* 29.

Huang, Z., Sheng, Z., Ma, C., Chen, S., 2024. Human as ai mentor: Enhanced human-in-the-loop reinforcement learning for safe and efficient autonomous driving. *Communications in Transportation Research* 4, 100127.

Jiang, Y., Jin, X., Xiong, Y., Liu, Z., 2020. A dynamic motion planning framework for autonomous driving in urban environments, in: 2020 39th Chinese Control Conference (CCC), IEEE. pp. 5429–5435.

Kakade, S., Langford, J., 2002. Approximately optimal approximate reinforcement learning, in: Proceedings of the Nineteenth International Conference on Machine Learning, pp. 267–274.

Kumar, A., Zhou, A., Tucker, G., Levine, S., 2020. Conservative q-learning for offline reinforcement learning. *Advances in Neural Information Processing Systems* 33, 1179–1191.

Kuznetsova, E., Li, Y.F., Ruiz, C., Zio, E., Ault, G., Bell, K., 2013. Reinforcement learning for microgrid energy management. *Energy* 59, 133–146.

Lee, S.E., Olsen, E.C., Wierwille, W.W., et al., 2004. A comprehensive examination of naturalistic lane-changes. Technical Report. United States. National Highway Traffic Safety Administration.

Li, G., Yang, Y., Li, S., Qu, X., Lyu, N., Li, S.E., 2022a. Decision making of autonomous vehicles in lane change scenarios: Deep reinforcement learning approaches with risk awareness. *Transportation research part C: emerging technologies* 134, 103452.

Li, N., Oyler, D.W., Zhang, M., Yildiz, Y., Kolmanovsky, I., Girard, A.R., 2017. Game theoretic modeling of driver and vehicle interactions for verification and validation of autonomous vehicle control systems. *IEEE Transactions on control systems technology* 26, 1782–1797.

Li, Q., Peng, Z., Zhou, B., 2022b. Efficient learning of safe driving policy via human-ai copilot optimization. arXiv preprint arXiv:2202.10341 .

Likmeta, A., Metelli, A.M., Tirinzoni, A., Giol, R., Restelli, M., Romano, D., 2020. Combining reinforcement learning with rule-based controllers for transparent and general decision-making in autonomous driving. *Robotics and Autonomous Systems* 131, 103568.

Liu, J., Qin, S., Su, M., Luo, Y., Zhang, S., Wang, Y., Yang, S., 2023. Traffic signal control using reinforcement learning based on the teacher-student framework. *Expert Systems with Applications* 228, 120458.

Liu, Z., Cen, Z., Isenbaev, V., Liu, W., Wu, S., Li, B., Zhao, D., 2022. Constrained variational policy optimization for safe reinforcement learning, in: *International Conference on Machine Learning*, PMLR. pp. 13644–13668.

Mnih, V., 2013. Playing atari with deep reinforcement learning. *arXiv preprint arXiv:1312.5602* .

Mo, S., Pei, X., Wu, C., 2021. Safe reinforcement learning for autonomous vehicle using monte carlo tree search. *IEEE Transactions on Intelligent Transportation Systems* 23, 6766–6773.

Mozina, M., Guid, M., Krivec, J., Sadikov, A., Bratko, I., 2008. Fighting knowledge acquisition bottleneck with argument based machine learning., in: *ECAI*, pp. 234–238.

Niaz, A., Shoukat, M.U., Jia, Y., Khan, S., Niaz, F., Raza, M.U., 2021. Autonomous driving test method based on digital twin: A survey, in: *2021 International Conference on Computing, Electronic and Electrical Engineering (ICE Cube)*, IEEE. pp. 1–7.

Ou, W., Luo, B., Wang, B., Zhao, Y., 2024. Modular hierarchical reinforcement learning for multi-destination navigation in hybrid crowds. *Neural Networks* 171, 474–484.

Patz, B.J., Papelis, Y., Pillat, R., Stein, G., Harper, D., 2008. A practical approach to robotic design for the darpa urban challenge. *Journal of Field Robotics* 25, 528–566.

Pendharkar, P.C., Cusatis, P., 2018. Trading financial indices with reinforcement learning agents. *Expert Systems with Applications* 103, 1–13.

Peng, B., Duan, J., Chen, J., Li, S.E., Xie, G., Zhang, C., Guan, Y., Mu, Y., Sun, E., 2022a. Model-based chance-constrained reinforcement learning via separated proportional-integral lagrangian. *IEEE Transactions on Neural Networks and Learning Systems* 35, 466–478.

Peng, Z., Li, Q., Liu, C., Zhou, B., 2022b. Safe driving via expert guided policy optimization, in: *Conference on Robot Learning*, PMLR. pp. 1554–1563.

Pomerleau, D.A., 1991. Efficient training of artificial neural networks for autonomous navigation. *Neural computation* 3, 88–97.

Qiao, Z., Muelling, K., Dolan, J.M., Palanisamy, P., Mudalige, P., 2018. Automatically generated curriculum based reinforcement learning for autonomous vehicles in urban environment, in: *2018 IEEE Intelligent Vehicles Symposium (IV)*, IEEE. pp. 1233–1238.

Sallab, A.E., Abdou, M., Perot, E., Yogamani, S., 2017. Deep reinforcement learning framework for autonomous driving. *arXiv preprint arXiv:1704.02532* .

Schulman, J., Levine, S., Abbeel, P., Jordan, M., Moritz, P., 2015. Trust region policy optimization, in: *International conference on machine learning*, PMLR. pp. 1889–1897.

Schulman, J., Wolski, F., Dhariwal, P., Radford, A., Klimov, O., 2017. Proximal policy optimization algorithms. *arXiv preprint arXiv:1707.06347* .

Shu, H., Liu, T., Mu, X., Cao, D., 2021. Driving tasks transfer using deep reinforcement learning for decision-making of autonomous vehicles in unsignalized intersection. *IEEE Transactions on Vehicular Technology* 71, 41–52.

Song, Y., Lin, H., Kaufmann, E., Dürr, P., Scaramuzza, D., 2021. Autonomous overtaking in gran turismo sport using curriculum reinforcement learning, in: *2021 IEEE international conference on robotics and automation (ICRA)*, IEEE. pp. 9403–9409.

Stooke, A., Achiam, J., Abbeel, P., 2020. Responsive safety in reinforcement learning by pid lagrangian methods, in: *International Conference on Machine Learning*, PMLR. pp. 9133–9143.

Subramanian, A., Chitlangia, S., Baths, V., 2022. Reinforcement learning and its connections with neuroscience and psychology. *Neural Networks* 145, 271–287.

Treiber, M., Hennecke, A., Helbing, D., 2000. Congested traffic states in empirical observations and microscopic simulations. *Physical review E* 62, 1805.

Tsantekidis, A., Passalis, N., Tefas, A., 2023. Modeling limit order trading with a continuous action policy for deep reinforcement learning. *Neural Networks* 165, 506–515.

Voogd, K.L., Allamaa, J.P., Alonso-Mora, J., Son, T.D., 2023. Reinforcement learning from simulation to real world autonomous driving using digital twin. *IFAC-PapersOnLine* 56, 1510–1515.

Wang, K., Yu, T., Li, Z., Sakaguchi, K., Hashash, O., Saad, W., 2024. Digital twins for autonomous driving: A comprehensive implementation and demonstration, in: *2024 International Conference on Information Networking (ICOIN)*, IEEE. pp. 452–457.

Wu, J., Huang, Z., Hu, Z., Lv, C., 2023. Toward human-in-the-loop ai: Enhancing deep reinforcement learning via real-time human guidance for autonomous driving. *Engineering* 21, 75–91.

Xue, Z., Peng, Z., Li, Q., Liu, Z., Zhou, B., 2023. Guarded policy optimization with imperfect online demonstrations. *arXiv preprint arXiv:2303.01728* .

Ye, D., Liu, Z., Sun, M., Shi, B., Zhao, P., Wu, H., Yu, H., Yang, S., Wu, X., Guo, Q., et al., 2020. Mastering complex control in moba games with deep reinforcement learning, in: *Proceedings of the AAAI Conference on Artificial Intelligence*, pp. 6672–6679.

Yu, L., Xie, W., Xie, D., Zou, Y., Zhang, D., Sun, Z., Zhang, L., Zhang, Y., Jiang, T., 2019. Deep reinforcement learning for smart home energy management. *IEEE Internet of Things Journal* 7, 2751–2762.

Yun, H., Park, D., 2021. Simulation of self-driving system by implementing digital twin with gta5, in: *2021 international conference on electronics, information, and communication (ICEIC)*, IEEE. pp. 1–2.

Zhang, F., Yang, Q., An, D., 2022a. A leader-following paradigm based deep reinforcement learning method for multi-agent cooperation games. *Neural Networks* 156, 1–12.

Zhang, W., Deng, L., Zhang, L., Wu, D., 2022b. A survey on negative transfer. *IEEE/CAA Journal of Automatica Sinica* 10, 305–329.

Zhang, X., Jiang, Y., Lu, Y., Xu, X., 2022c. Receding-horizon reinforcement learning approach for kinodynamic motion planning of autonomous vehicles. *IEEE Transactions on Intelligent Vehicles* 7, 556–568.

Zhang, Z., Liu, Q., Li, Y., Lin, K., Li, L., 2024. Safe reinforcement learning in autonomous driving with epistemic uncertainty estimation. *IEEE Transactions on Intelligent Transportation Systems* .

Zhou, R., Cao, H., Huang, J., Song, X., Huang, J., Huang, Z., 2024. Hybrid lane change strategy of autonomous vehicles based on soar cognitive architecture and deep reinforcement learning. *Neurocomputing* , 128669.

Zhu, Z., Zhao, H., 2021. A survey of deep rl and il for autonomous driving policy learning. *IEEE Transactions on Intelligent Transportation Systems* 23, 14043–14065.

Zimmer, M., Viappiani, P., Weng, P., 2014. Teacher-student framework: a reinforcement learning approach, in: *AAMAS Workshop autonomous robots and multirobot systems*.

A Proof of Theorem 3

Theorem 5 (Restatement of Theorem 3). *With the switch function, the return of the mixed behavior policy $J(\theta_{\text{mix}})$ is lower and upper bounded by:*

$$J(\theta_t) + \frac{\sqrt{2}(1-\omega)R_{\max}}{(1-\gamma)^2} \sqrt{H-\kappa} \geq J(\theta_{\text{mix}}) \geq J(\theta_t) - \frac{\sqrt{2}(1-\omega)R_{\max}}{(1-\gamma)^2} \sqrt{H-\kappa} \quad (33)$$

Proof. Using the mixed behavior policy as defined in Eq. 19, the difference between $J_{\theta_{\text{mix}}}$ and the return of the teacher’s policy J_{θ_t} , is expressed as follows:

$$\begin{aligned} |J(\theta_{\text{mix}}) - J(\theta_t)| &\leq \frac{R_{\max}}{(1-\gamma)^2} \mathbb{E}_{s \sim d_{\text{mix}}} \|\pi^{\text{mix}}(\cdot|s) - \pi^t(\cdot|s)\|_1 \\ &= \frac{R_{\max}}{(1-\gamma)^2} \mathbb{E}_{s \sim d_{\text{mix}}} \|\mathcal{T}(s)\pi^t(\cdot|s) + (1-\mathcal{T}(s))\pi^s(\cdot|s) - \pi^t(\cdot|s)\|_1 \\ &= \frac{(1-\omega)R_{\max}}{(1-\gamma)^2} \mathbb{E}_{s \sim d_{\text{mix}}} \|\pi^s(\cdot|s) - \pi^t(\cdot|s)\|_1 \\ &\leq \frac{\sqrt{2}(1-\omega)R_{\max}}{(1-\gamma)^2} \mathbb{E}_{s \sim d_{\text{mix}}} \sqrt{D_{\text{KL}}(\pi^t(\cdot|s) \parallel \pi^s(\cdot|s))} \\ &= \frac{\sqrt{2}(1-\omega)R_{\max}}{(1-\gamma)^2} \mathbb{E}_{s \sim d_{\text{mix}}} \sqrt{\mathbb{E}_{a \sim \pi^t(\cdot|s)} \left[\log \frac{\pi^t(a|s)}{\pi^s(a|s)} \right]} \\ &= \frac{\sqrt{2}(1-\omega)R_{\max}}{(1-\gamma)^2} \mathbb{E}_{s \sim d_{\text{mix}}} \sqrt{\mathcal{H}(\pi^t(\cdot|s)) - \kappa} \\ &\leq \frac{\sqrt{2}(1-\omega)R_{\max}}{(1-\gamma)^2} \sqrt{H-\kappa}. \end{aligned} \quad (34)$$

So we can obtain:

$$\begin{aligned} \frac{\sqrt{2}(1-\omega)R_{\max}}{(1-\gamma)^2}\sqrt{H-\kappa} &\geq J(\theta_{\text{mix}}) - J(\theta_t) \geq -\frac{\sqrt{2}(1-\omega)R_{\max}}{(1-\gamma)^2}\sqrt{H-\kappa} \\ J(\theta_t) + \frac{\sqrt{2}(1-\omega)R_{\max}}{(1-\gamma)^2}\sqrt{H-\kappa} &\geq J(\theta_{\text{mix}}) \geq J(\theta_t) - \frac{\sqrt{2}(1-\omega)R_{\max}}{(1-\gamma)^2}\sqrt{H-\kappa} \end{aligned} \quad (35)$$

Proof completed.

B Proof of Theorem 4

Theorem 6 (Restatement of Theorem 4). *The expected cumulative reward obtained by learning from π^{mix} is guaranteed to be greater than or equal to the expected cumulative reward obtained by the π^t :*

$$\mathbb{E}_{\pi^{\text{mix}}}\left[\sum_{t=0}^H \gamma^t r(s_t, a_t)\right] \geq \mathbb{E}_{\pi^t}\left[\sum_{t=0}^H \gamma^t r(s_t, a_t)\right] \quad (36)$$

Proof. We will prove this using the method of induction. When $H = 0$, according to the switch function, the mixed policy π^{mix} will choose the action that results in the highest reward:

$$\mathbb{E}_{\pi^{\text{mix}}}[r(s, a)] = \max(\mathbb{E}_{\pi^t}[r(s, a)], \mathbb{E}_{\pi^s}[r(s, a)]) \quad (37)$$

Now, assume that the theorem holds for some horizon $k \geq 0$:

$$\mathbb{E}_{\pi^{\text{mix}}}\left[\sum_{t=0}^k \gamma^t r(s_t, a_t)\right] = \max\left(\mathbb{E}_{\pi^t}\left[\sum_{t=0}^k \gamma^t r(s_t, a_t)\right], \mathbb{E}_{\pi^s}\left[\sum_{t=0}^k \gamma^t r(s_t, a_t)\right]\right) \quad (38)$$

With this assumption in place, we need to demonstrate that the theorem holds for the horizon $k + 1$. To achieve this, define the value function for the policy π as:

$$V_{\pi}(s) = \mathbb{E}_{\pi}\left[\sum_{t=0}^{k+1} \gamma^t r(s_t, a_t) \mid s_0 = s\right] = r(s, \pi(s)) + \gamma \mathbb{E}_{s' \sim P(s'|s, \pi(s))}[V_{\pi}(s')] \quad (39)$$

For π^{mix} , this equation becomes:

$$V_{\pi^{\text{mix}}}(s) = \max(r(s, \pi^t(s)) + \gamma \mathbb{E}_{s'}[V_{\pi^{\text{mix}}}(s')], r(s, \pi^s(s)) + \gamma \mathbb{E}_{s'}[V_{\pi^{\text{mix}}}(s')]) \quad (40)$$

By the inductive hypothesis, we know that $V_{\pi^{\text{mix}}}(s') = \max(V_{\pi^t}(s'), V_{\pi^s}(s'))$ for all s' . Substituting this into the above equation:

$$\begin{aligned} V_{\pi^{\text{mix}}}(s) &= \max(r(s, \pi^t(s)) + \gamma \mathbb{E}_{s'}[\max(V_{\pi^t}(s'), V_{\pi^s}(s'))], r(s, \pi^s(s)) + \gamma \mathbb{E}_{s'}[\max(V_{\pi^t}(s'), V_{\pi^s}(s'))]) \\ &\geq \max(r(s, \pi^t(s)) + \gamma \mathbb{E}_{s'}[(V_{\pi^t}(s'))], r(s, \pi^s(s)) + \gamma \mathbb{E}_{s'}[(V_{\pi^s}(s'))]) \\ &= \max(V_{\pi^t}(s), V_{\pi^s}(s)) \\ &\geq V_{\pi^t}(s) \end{aligned} \quad (41)$$

This result demonstrates that the theorem holds for horizon $k + 1$. By the principle of mathematical induction, we can conclude that the theorem holds for all finite horizons $H \geq 0$. Thus, the hybrid policy π^{mix} outperforms the existing physics-based policy π^t , namely:

$$\mathbb{E}_{\pi^{\text{mix}}}\left[\sum_{t=0}^H \gamma^t r(s_t, a_t)\right] \geq \mathbb{E}_{\pi^t}\left[\sum_{t=0}^H \gamma^t r(s_t, a_t)\right] \quad (42)$$

Proof completed.

C Hyper-parameters

Hyper-parameters of different baseline algorithms.

Table 12: PPO/PPO-Lag

Hyper-parameters	Value
Maximal learning rate	0.0005
Learning rate decay	True
Total steps of one episode	5,000
Total training steps	500K
Optimizer	Adam W
Mini batch size	64
Discount factor γ	0.96
Lambda entropy β	0.01
Clip parameter ϵ	0.2
Lambda advantage λ	0.98
Penalty parameter	0.2
Cost limit for PPO-Lag	0

Table 13: SAC/SAC-Lag/CQL

Hyper-parameters	Value
Maximal learning rate	0.0005
Learning rate decay	True
Total steps of one episode	5,000
Total training steps	500K
Optimizer	Adam W
Mini batch size	64
Discount factor γ	0.96
Buffer size	1e6
Temperature parameter ν	-2
Learning rate of α	0.001
Target entropy	-1
Penalty parameter	0.2
Cost limit for SAC-Lag	0
Dataset Size	1e6
CQL loss temperature	3
Min Q weight multiplier	0.2

Table 14: GAIL/BC

Hyper-parameters	Value
Maximal learning rate	0.0005
Learning rate decay	True
Total steps of one episode	5,000
Total training steps	500K
Optimizer	Adam W
Mini batch size	64
Discount factor γ	0.96
Dataset Size	40 K
Sample batch size	5,000
Discriminator learning rate	0.001

Table 15: DQN

Hyper-parameters	Value
Maximal learning rate	0.0005
Learning rate decay	True
Total steps of one episode	5,000
Total training steps	500K
Optimizer	Adam W
Mini batch size	64
Discount factor γ	0.96
Buffer size	1e6
Explore rate of ϵ -greedy	0.25

Table 16: TS2C

Hyper-parameters	Value
Maximal learning rate	0.0005
Learning rate decay	True
Total steps of one episode	5,000
Total training steps	500K
Optimizer	Adam W
Mini batch size	64
Discount factor γ	0.96
Lambda entropy β	0.01
Clip parameter ϵ	0.2
Lambda advantage λ	0.98
Intervention Threshold ε'	0.5
Intervention Minimization Ratio	1

Table 17: SOAR-ACPPO

Hyper-parameters	Value
Hyperparameter q_1	5
Hyperparameter q_2	10
Maximal learning rate	0.0005
Learning rate decay	True
Total steps of one episode	5,000
Total training steps	500K
Optimizer	AdamW
Mini batch size	64
Discount factor γ	0.96
Lambda entropy β	0.01
Clip parameter ϵ	0.2
Lambda advantage λ	0.98
Hyperparameter of AC ψ	0.2